DESIGN AND CONSTRUCTION OF A SHOCK TUBE

FACILITY FOR THE STUDY OF SHOCK

WAVES EMERGING FROM OPENINGS

By

GLENDON RAY LAZALIER

Bachelor of Science

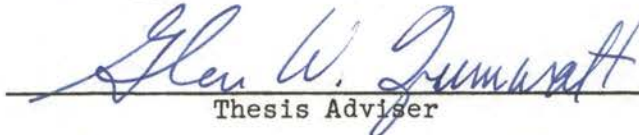Oklahoma State University

Stillwater, Oklahoma

1963

Submitted to the Faculty of the Graduate School
of the Oklahoma State University of
Agriculture and Applied Sciences
in partial fulfillment of
the requirements of
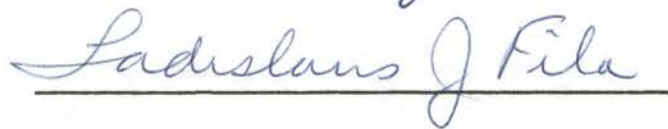MASTER OF SCIENCE
May, 1965

DESIGN AND CONSTRUCTION OF A SHOCK TUBE

FACILITY FOR THE STUDY OF SHOCK

WAVES EMERGING FROM OPENINGS

Thesis Approved:

_____
Thesis Adviser

_____

_____
Dean of the Graduate School

ii

PREFACE

Whenever a body travels at a speed greater than the local acoustic velocity the body causes shock waves to exist in the surrounding flow. The close passage of two such supersonic bodies or the passage of such a body through a pressure disturbance traveling at a velocity greater than the local acoustic velocity may cause complex wave interactions. These interactions will be functions of the velocity, size, shape and material of both the interacting media.

To study fully the problems of the interactions of such bodies requires certain experimental verification of theoretical results. There are many schemes which may be used with varying degrees of success to achieve these ends. One such scheme is to produce a supersonic pressure disturbance and cause it to interact with bodies and other disturbances. This may be achieved by utilizing a shock tube to produce shock fronts which then interact with other shock fronts and bodies. Of paramount importance in the use of this scheme is a complete knowledge of the behavior of the shock front as it emerges from the shock tube and either separately or simultaneously interacts with the various media under investigation. The facility described in this study has been designed to carry out investigations of the above happenings. This study was sponsored by Sandia Corporation of Albuquerque, New Mexico.

iii

TABLE OF CONTENTS

LIST OF TABLES

LIST OF FIGURES

LIST OF PLATES

CHAPTER I

INTRODUCTION

At low altitudes, the energy of an exploding nuclear or other high-yield explosive device is released in two forms: heat and an approximately spherical pressure disturbance. The radiant heat energy is propagated at the velocity of light and its intensity at any point is inversely proportional to the square of the distance from the point to the point of the explosion. The pressure disturbance expands in a spherical (for ideal, homogenous gases) manner with a velocity greater than the local acoustic velocity. This velocity may easily reach ten to twenty times the local acoustic velocity. The fireball portion of the heat energy expands more slowly than the pressure disturbance and, consequently, expands through a gas which has had its properties altered.

As the pressure disturbance proceeds through the gas, it compresses, heats, and accelerates the ambient gas. The degree of compression, heating, and acceleration of the air are well known from classical gas dynamics relationships, (Rankine-Hugoniot relations). For very high pressure disturbance velocities relative to the local acoustic velocity the air may become both disassociated and ionized. However, these effects may be neglected for values of the Mach number less than five.

1

Upon reaching a solid surface the pressure disturbance (hereafter called "blast wave" or "shock wave") is reflected. As it proceeds back through the air it has compressed, heated, and accelerated, the shock further compresses and heats the air with the ensuing acceleration opposing the previous acceleration. As a result of the second compression and heating the air is very nearly motionless with the pressures and temperatures on the exposed sides of the object greatly in excess of those on the unexposed sides (see Appendix A for analysis of resulting pressures and temperatures). Consequently, large forces and aerodynamic moments may be caused to exist on bodies passing through a blast wave. These forces and moments can cause attitude disturbances, control difficulties, and even catastrophic failure of surface areas of the body. The following figure (Figure 1) shows a possible configuration in a representative time-event portrayal.

The effect on a body of the steady state flow pattern existing behind a blast wave has been reported by Dowlen and others. Of paramount importance, however, is the effect of the actual missile shock wave and blast wave interactions on the flow field surrounding the missile. Work is presently underway at Oklahoma State University by Mssrs. Lynn D. Tyler, William F. Walker, and William N. Jackomis to achieve analytical solutions to this problem.

Two separate approaches have been suggested to determine experimentally the interaction relations of a missile flow field and a blast wave. These methods are:

(1) ballistic missile ranges intersected by shock

tubes and
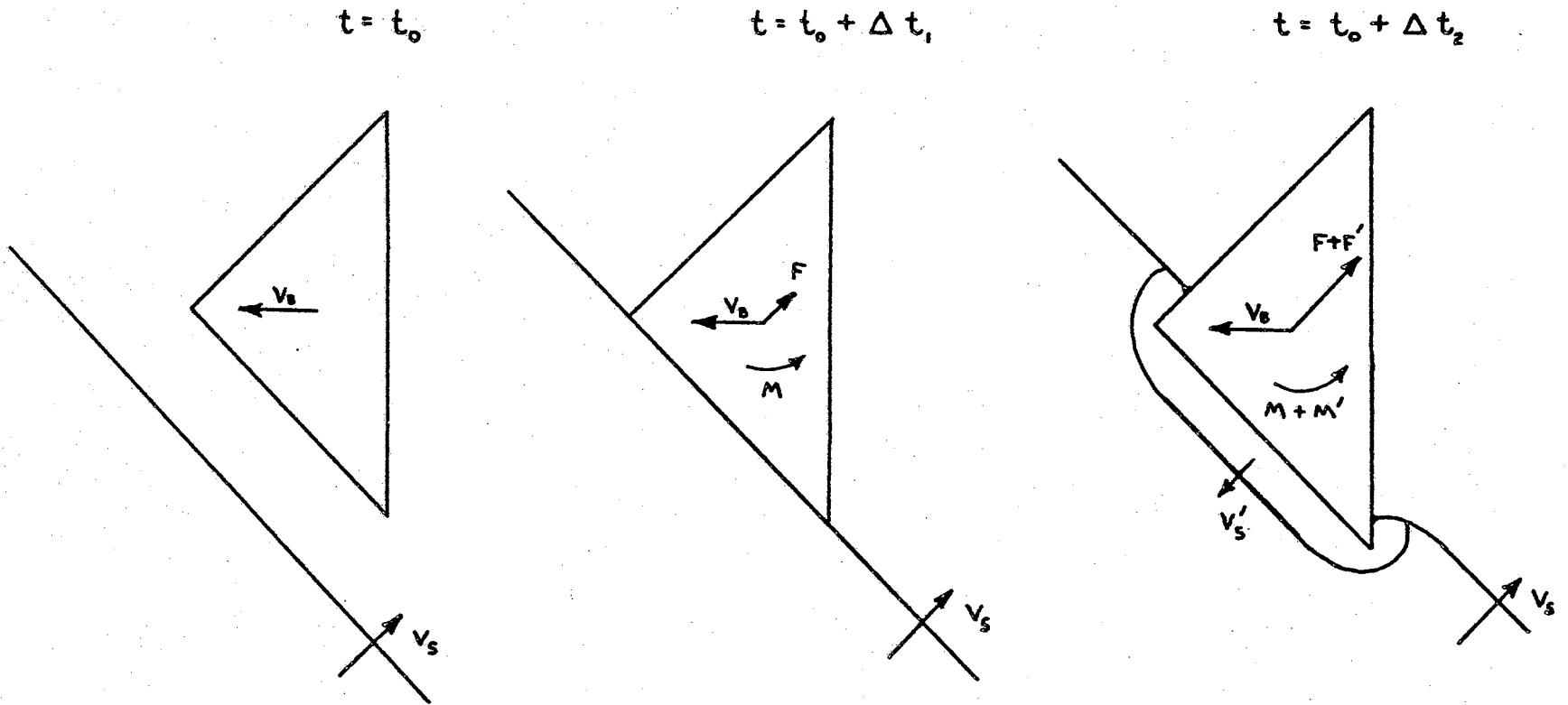
Figure 1. Impacting of Shock Wave on Slow-Moving Body.

(2)   supersonic wind tunnels with side-mounted

shock tubes.

The instrumentation is considerably more difficult and the space required for the successful operation is much greater for the first method than for the second.

Utilization of the approach to the problem suggested by the second of the two above methods reveals the presence of three related problems. These problems are:

(1)   behavior of a plane shock leaving a shock tube

of general cross sectional geometry and passing

into a still semi-infinite medium,

(2)   behavior of a shock in passing through a jet

mixing region, and

(3)   behavior of a shock in passing into a supersonic

stream.

The solutions of (2) and (3) above are being undertaken by Mssrs. Tyler and Walker.

Background

Most shock tube studies of the past have been concerned with behavior within the shock tube itself (1, 2, 3).[1] However, Elder and de Haas (4), Lee (5), and Pierce (6) have been concerned with the behavior of the shock front as it passed from the tube into a semi-infinite medium.

---

[1]Note: Numbers in parentheses, after names, refer to numbered references in Selected Bibliography.

In these cases the study has used a weak shock and/or a free expansion of the shock front caused by allowing it to turn through 180° as it leaves the tube. The facilities designed to accomplish the above work have not focused attention on the behavior of a strong shock front as it turns through a restricted angle after leaving the tube. The above papers have been concerned with such things as the vortex rings formed and the effects of the shock on objects in its path.

Other authors, such as Bingham and Davidson (7), have established results for shock-shock interactions but have neglected the behavior of a shock front as it passes into a restricted expansion area. The behavior of a shock front as it passes a turn of a given angle on the overall effect and strength of the shock front is a critical factor in the successful operation of an experimental facility to determine the behavior and interaction of shocks with other shocks and with missile flow fields. The need for experimental verification of theories of emerging shock behavior and shock-shock interactions lead to this work.

Purpose

The purpose of this study is twofold:

(1) Design, construct, and establish operating procedures for a short shock tube capable of producing shock waves with Mach numbers of approximately two to three and

(2) devise suitable techniques for the determination of the behavior of the emerging shock fronts.

The shock tube will be somewhat unique in that it has a length/diameter ratio of only twelve and relies on a double diaphragm configuration to obtain clean shock waves.

Method of Approach

To accomplish the two part purpose set out above the following steps were undertaken:

(1) Utilization of a perfect gas analysis was made to establish a design point for an experimental shock tube configuration.

(2) Selection of materials and fabrication of a shock tube to operate about the design point obtained in (1) was accomplished.

(3) Safe operating procedures for the shock tube were established which enabled it to be used to determine the second portion of the purpose of this study.

(4) Installation of sufficient measurement devices to verify the actual performance of the shock tube compared to the theoretical performance was made.

(5) Methods were devised to determine experimentally the behavior of emerging shock waves.

(6) Conclusions concerning the effectiveness of the facility were drawn.

CHAPTER II

SHOCK TUBE DESIGN

Basic Design

The basic design of the required shock tube assembly was determined from a perfect gas analysis (see Appendix A). In order to obtain a higher level of performance and to utilize a ready source of high pressure driver gas, unheated helium was chosen as the driver gas. The helium used as the supply source was obtained in two and one-half cubic feet bottles at approximately 1800 pounds per square inch gage. Helium further had the desirable properties of being non-toxic and non-explosive. Rarified air was chosen as an expedient driver gas because the ratio of molecular weights of helium and air is beneficial to high performance.

An attempt was made during the design of the shock tube to achieve an unusually short assembly to:

(1) prevent the reflected rarefaction wave from over-taking the shock wave,

(2) reduce boundary layer effects in the flow behind the shock,

(3) conserve laboratory space, and

(4) provide a short shock tube facility for demonstration purposes.

Final choices of lengths were a one-foot driver section, a three-foot driven section, and a four inch intermediate section of which one and five-eighths inch separated the diaphragms in a double diaphragm arrangement. These lengths are such that the rarefaction wave which proceeds upstream from the bursting diaphragm will not, after reflection, overtake the initial shock wave as it proceeds downstream before the shock has emerged from the end. The dimensions of the intermediate section will be explained in a later section of this study.

It has been reported by Lee, et al (1) that the reflected rarefaction wave should just overtake the initial shock wave at the test section in order to produce a realistic blast wave profile. Since, however, the major concern of this paper was to construct a facility to determine the behavior of an emerging plane shock wave as it leaves various geometrical openings, and since most available shock tubes produce shock waves which are unaffected by the reflected rarefaction wave, this method was not chosen. Further, the production of such artificial blast wave profiles requires a test facility which possesses a high degree of exact repeatability. It was felt that the use of pressure burst diaphragms (a necessary factor in short tubes because of the disturbances produced by plungers and shaped charges) limited the repeatability of the facility to the extent of ruling out such test procedures.

The shock tube proper was constructed of 3.00 inch inner diameter hydraulic tubing extruded from mild steel. The nominal wall thickness of the hydraulic tubing was three-eighths inch. Hydraulic tubing was selected as the construction material because:

(1) the seamless configuration provided great structural

strength,

(2) the inside walls could be obtained in a very smooth

condition which precluded further honing, and

(3) the material was readily obtainable commercially.

The details of the method selected for joining the driver, driven, and intermediate sections are shown in Figure 2. The flanges selected were 600 pound schedule forged steel ASA flanges. The proper portion of each section of the driver and driven sections of the shock tube were joined to the flanges with a one-half inch fillet arc weld. The flanges were joined across the intermediate section by eight three-quarters inch UNC bolts eight inches long. The intermediate section was kept in proper alignment by a 5 3/4 inch I. D. cylindrical sleeve as shown in Figure 2. During operations the bolts were torqued to a minimum of 200 foot-pounds to insure complete sealing.

A pressure ratio (P_{driver}/P_{driven}) of about 100:1 was selected as the design point of the shock tube. This pressure ratio gives a Mach number of 1.5 to 3.6, depending on the ratio of driver to intermediate pressures, for the shock front when subjected to a perfect gas analysis (Appendix A). To achieve this ratio the driver section was designed for a working pressure of 400 psia. (Hydro-static tests were run at 800 psia to provide a large margin of safety.) By operating the driven section at 4.00 psia the desired ratio of 100:1 was obtained.

A maximum safe, workable ratio of 200:1 is considered to be the upper limit of operation. This ratio is obtained by lowering the pressure of the driven section to 2.0 psia and operating the driver section at 400 psia.
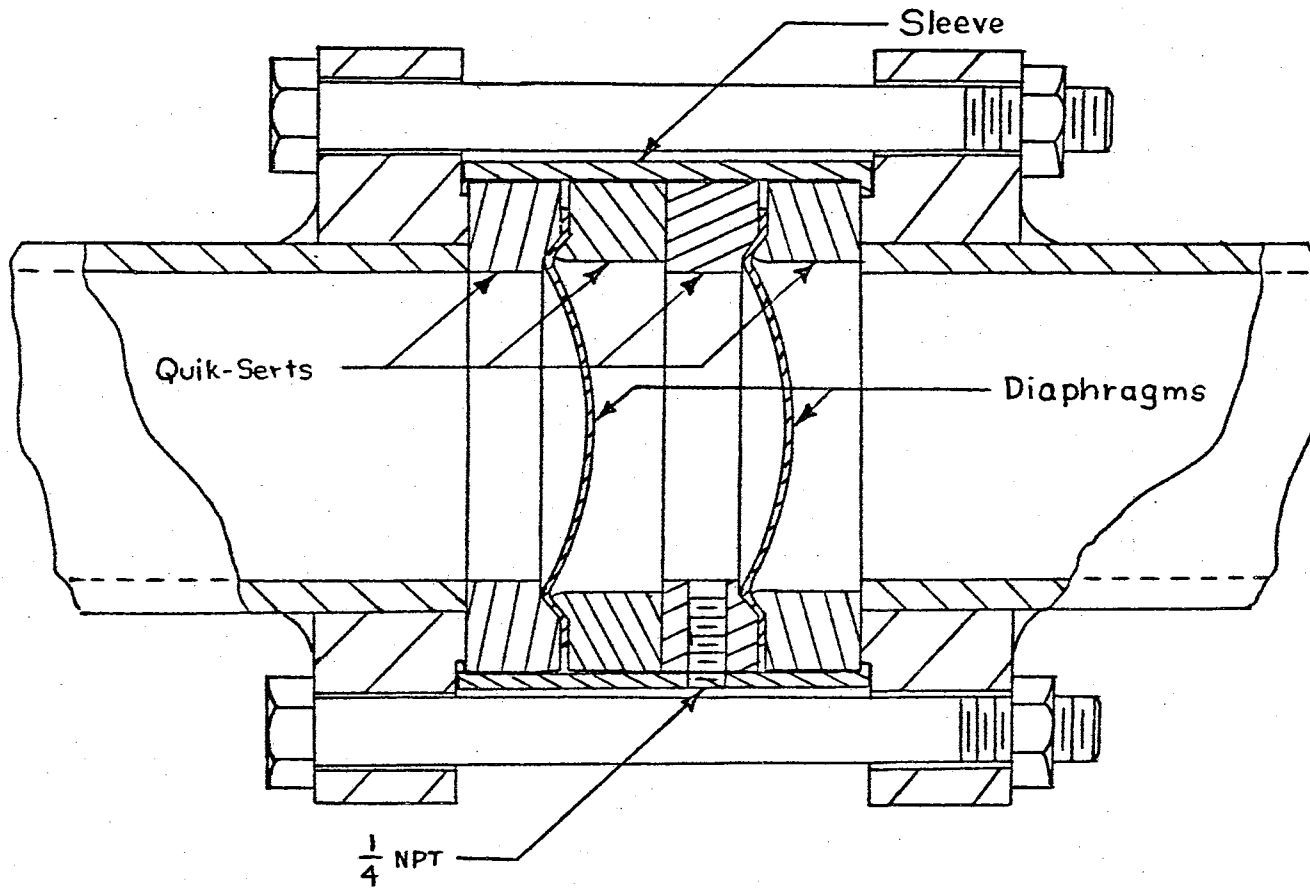
Figure 2. Details of Intermediate Section.

The limitation could be caused by density considerations for the schlieren system or by the error introduced by instrument inaccuracies.

Figure 3a shows the range of the ratio of (P_{driver}/P_{driven}) actual to $(P_{driver}/P_{driven})_{desired}$ for a nominal driver pressure of 400 psia and an instrument inaccuracy as follows.

$$P_{driver} \quad error \quad \pm \quad 2.0 \quad psi$$
$$P_{driven} \quad error \quad \pm \quad 0.05 \quad psi$$

Figure 3b indicates the range of shock strength (commonly P_2/P_1) for the above conditions.

Analysis of these figures indicates a practical engineering limit of 2.0 psia as the minimum driven pressure.

A quick check of schlieren requirements shows the following.

$$\lambda \equiv \text{mean free path length}$$
$$p \equiv \text{pressure of a perfect gas}$$
$$n \equiv \text{number of molecules per unit volume}$$

From kinetic theory;

$$\lambda \propto \frac{1}{n} \quad \text{and} \quad n \propto p$$

$$\therefore \lambda \propto \frac{1}{p}$$

Experimental evidence given by many references indicates that the thickness of a shock wave is a few mean free path lengths. The mean free path length for air at one atmosphere of pressure is 10^{-6} feet or less. Assuming the shock wave in air to be 5×10^{-6} feet and defining δ as
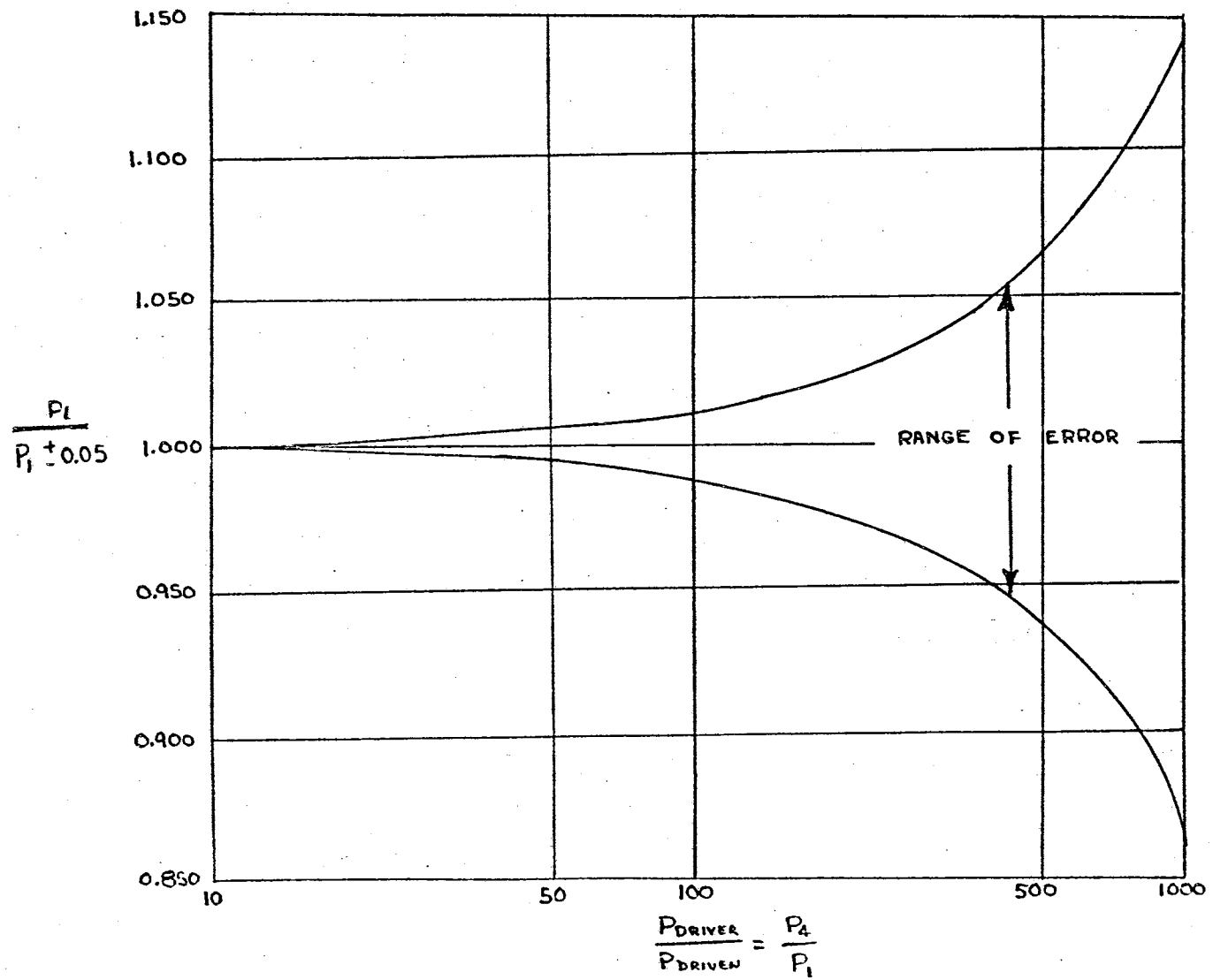
Figure 3a. Range of Total Error for Fixed Error in Reading Vacuum Gage.
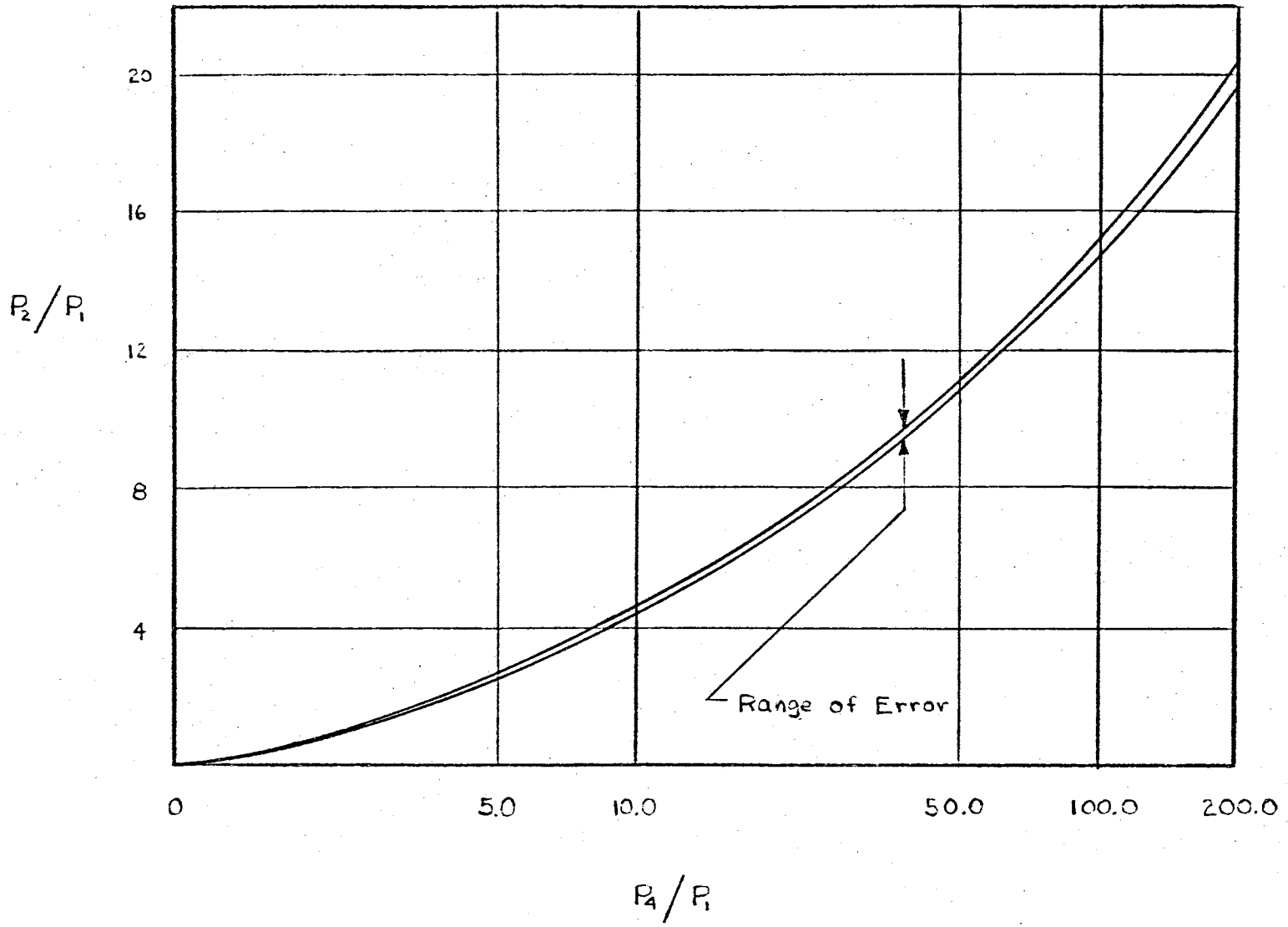
Figure 3b. Range of Error in Shock Strength.

the shock thickness results in the following.

$$\frac{\lambda_1}{\lambda_x} = \frac{P_x}{P_1} = \frac{\delta_1}{\delta_x} \qquad \text{where the subscripts refer to atmospheres of pressure}$$

$$\therefore \quad P_x = \frac{\delta_1}{\delta_x} (P_1)$$

From photographic considerations, schlieren systems may be successfully employed for $\delta < 4.33 \times 10^{-4}$ feet. Below this value the resulting photographs appear blurred.

$$P_x = \frac{\delta_x}{\delta_1} (P_1) = \left(\frac{4.33 \times 10^{-4}}{5.00 \times 10^{-6}} \right) \ 14.5 = 0.169 \text{ psia}$$

The minimum driven section pressure for schlieren operation is seen to be approximately 0.17 psia which indicates that the system is limited by instrument inaccuracies.

A double diaphragm configuration was selected to aid in the maintenance of repeatability of the experimental facility. Because of a desire to form shocks quickly, the use of plungers or shaped charges was ruled out as explained previously. Pressure burst diaphragms cause greater difficulties in breaking at a given differential than either of the above methods. However, the use of a double diaphragm configuration allowed the actual pressure differential necessary to operate the tube to be divided into two smaller differentials.

The shock tube consists of the three sections previously mentioned (driver, intermediate, and driven). By maintaining a pressure in the intermediate section equal to a specific fraction of the pressure in the driver section, the use of thinner diaphragms is permitted. These

thinner diaphragms result in better "petalling" of the diaphragms than
would be possible with one thick diaphragm. Because of the better
"petalling" of the diaphragms the subsequent flow is less restricted.
This less restricted flow allows the formation of a uniform shock front
with a minimum of time and, consequently, distance down the driven section
for the formation of the shock front is also minimized. This was one of
the design goals of the shock tube assembly.

By breaking the upstream (nearest to driver section) diaphragm first,
a sudden pressure rise is applied to the downstream diaphragm. This
sudden pressure rise is assumed to be a partially formed shock front.
As it proceeds down the tube it strikes the downstream diaphragm and is
reflected. The reflection of the partially formed shock front may cause
the shock formed when the downstream diaphragm breaks to be stronger for
certain operating conditions than it would be if only the pressure ratio
of driver to driven were used across a single diaphragm. This increase
in strength is caused by the increased stagnation pressure and temperature
which exist behind the reflected shock wave. However, in this particular
application, reflected shock theory predicts a decrease in performance
(see Appendix A, Section 2). The processes outlined above are shown in
Figure 4. Pictures of upstream and downstream diaphragms after burst may
be found in Plate I.

The above sequence of events is obtained by venting helium from the
intermediate chamber until the differential pressure acting on the upstream
diaphragm exceeds its burst pressure. When using this technique care
must be taken to reduce venting mass flow rate and surge volume. This was
accomplished in the facility by using a very small flow opening (0.02 inches)
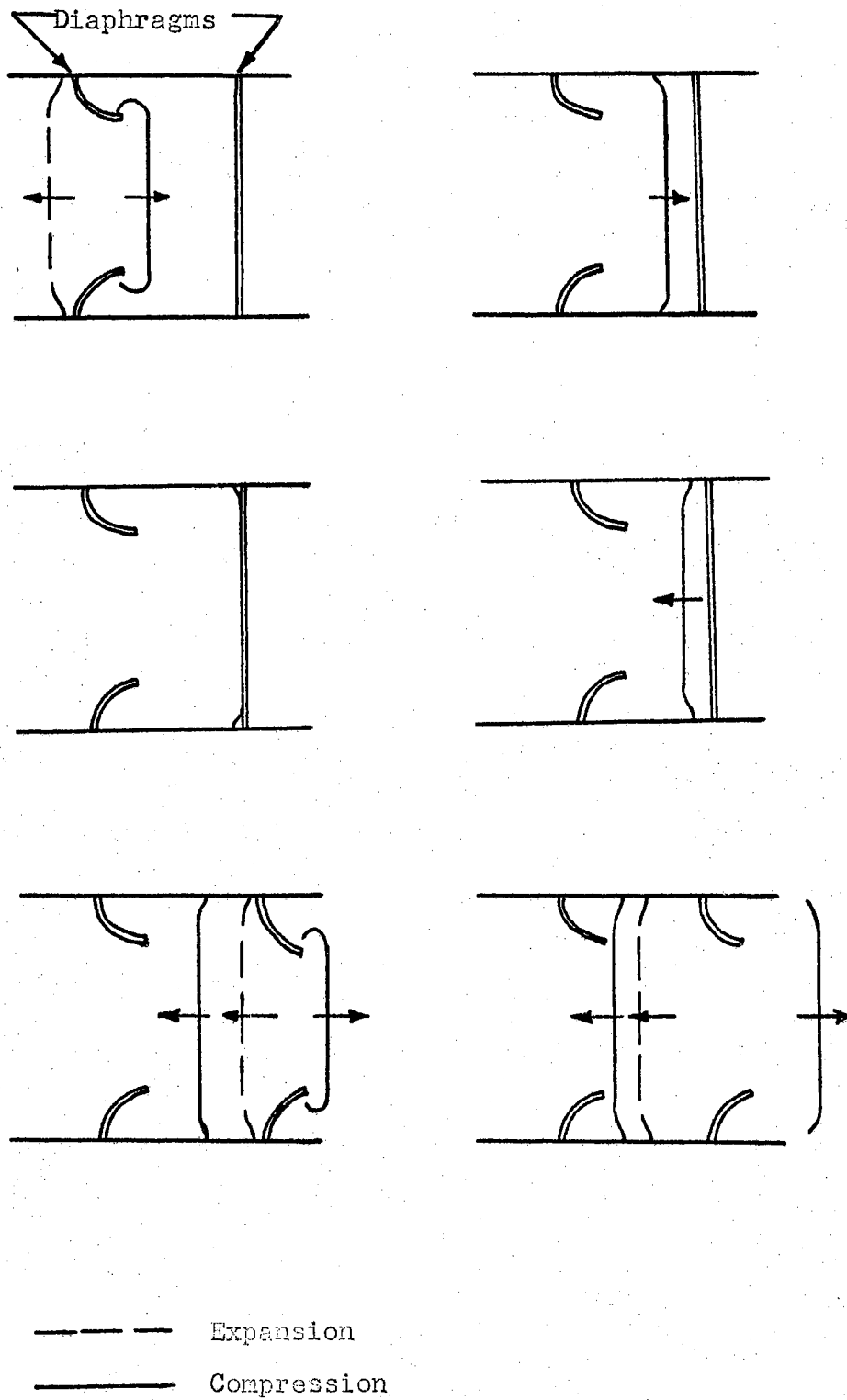
Figure 4. Physical Picture of Reflected Shock.

and a short, small diameter (0.06 inches) vent tube. An alternate procedure is to bring both driver and intermediate sections to the desired intermediate section pressure, close off the intermediate section and raise the driver pressure until burst occurs. All pressures at the time of the break are observed and recorded.

A graph of the location of the shock in the above processes and a graph of the location of the shock in a process which breaks the downstream diaphragm first are shown in Figure 5.

The actual Mach number of a shock wave in a conventional single diaphragm shock tube is always less than that predicted by a perfect gas analysis. Reasons for this discrepancy include viscous effects, imperfect diaphragm opening, energy to deflect the diaphragm, and related effects. In like manner, utilizing the technique described in Appendix A, Section III (double diaphragm, reflected shock, perfect gas), gives results higher than experimental values. A comparison of theory and experimental data may be found in Figure 13b.

Auxiliary Equipment

An attempt was made to use fully annealed aluminum diaphragms, 0.040 inch thick, fabricated by the author. Various scoring patterns used are illustrated in Figure 6. All methods left 0.005 to 0.020 inch thickness of metal in scored locations. Much difficulty was experienced in maintaining a uniform thickness which led to unpredictable diaphragm burst and insufficient "petalling" of the diaphragms.
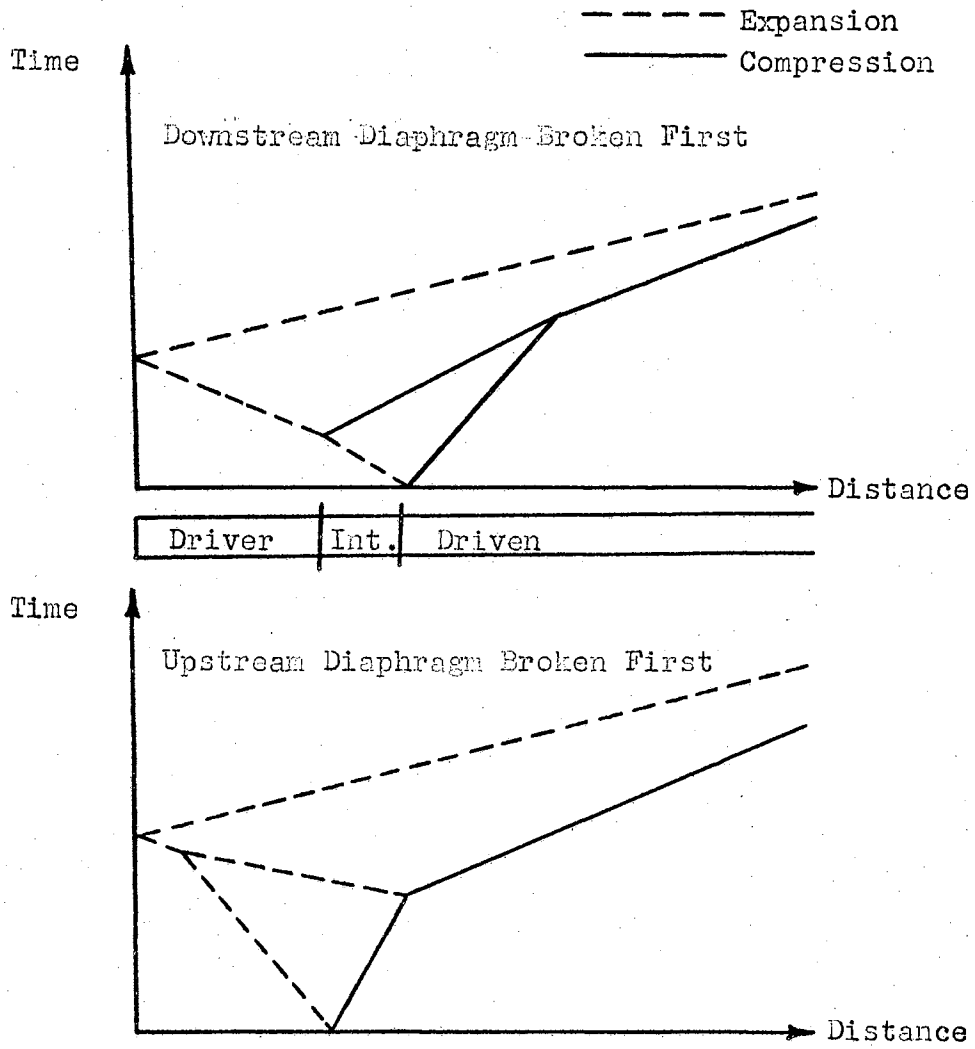
Figure 5. Time-Distance Plot for Shock Tube.
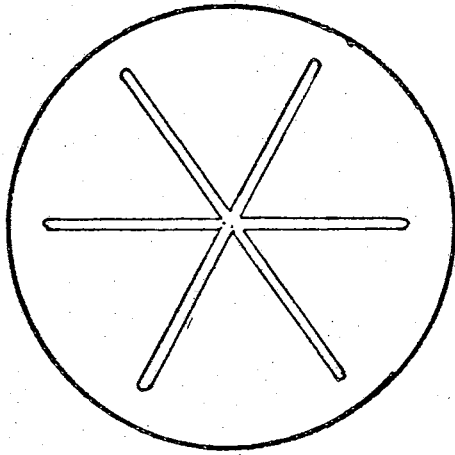
PRODUCED BY METHOD 1   PRODUCED BY METHOD 2
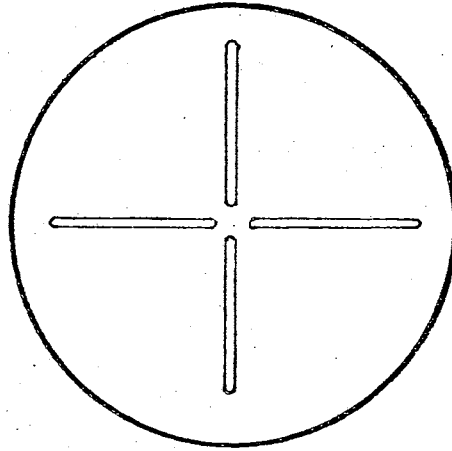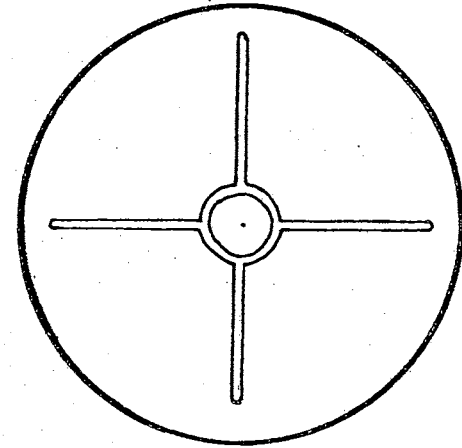
Figure 6. Experimental Diaphragms.

Two processes were devised to accomplish the scoring of the diaphragms mentioned above to improve the accuracy. The first consisted of a scribe mounted on sliding blocks with a threaded advance. In this process the metal was sheared with some actual removal of excess metal. The method led to rough spots and locally unsymmetrical strengths of the metal.

The second method utilized a press with a steel die. The dies were accurately machined to shape and used to impress their shape in the diaphragms. A constant force was applied to the die to produce even penetration. This method produced diaphragms which were better than the first process mentioned but which still did not provide the degree of accuracy required. It is felt that the local failure of parts of the diaphragms due to tearing caused by the die led to the failure of the method.

Finally it was decided to go to an outside source for diaphragms. The diaphragms selected were 3.00 inch diameter monel, scored safety discs made by Black, Sivalls & Bryson of Kansas City, Missouri. A rupture strength of 250 pounds per square inch differential with manufacturing tolerances of $+$ 10% and $-$ 5% was specified. The actual value of the average burst strength of the lot supplied was stamped on each diaphragm and this number was guaranteed within a plus or minus 5% when used with the "Quik-Serts" shown in Figure 2. Experimental variations of less than plus or minus 3% were experienced.

The receiver selected for the assembly was a commercially available ten inch cast steel tee section. The strength of the tee was much in excess of that required by the shock tube assembly. The tee was selected to provide a large mass to counteract the impulse applied to assembly when

the diaphragms broke. This impulse force is estimated to be equal to approximately twice the product of the burst pressure and the area of the diaphragms (8).

Blind flanges were turned to accomodate ten-inch windows on the crossbar of the tee. One-half inch plate glass of the first quality was used for these windows. These windows were sealed with Parker O-Rings. A third blind flange was turned to accomodate the shock tube proper which was then attached to the tee with one-half inch studs. The shock tube was sealed to the tee assembly with a sliding O-Ring arrangement shown in Figure 7. An overall view of the assembly is shown in Figure 8.

In order to utilize existing schlieren mirrors and knife edges for future optical studies the entire structure was mounted on a bench con- structed of one and one-half inch black iron pipe. This bench raises the centerline of the shock tube to approximately five feet and five inches from the floor. It also provided an assembly at a convenient height and made it accessible for modifications from all angles. Care was taken in the design of the bench to insure rigidity to reduce all unwanted motion to a minimum.

The pressure in the receiver chamber was maintained by a Welch Duo-Seal vacuum pump. Immediately prior to rupture of the diaphragms the vacuum pump was sealed off from the receiver chamber.
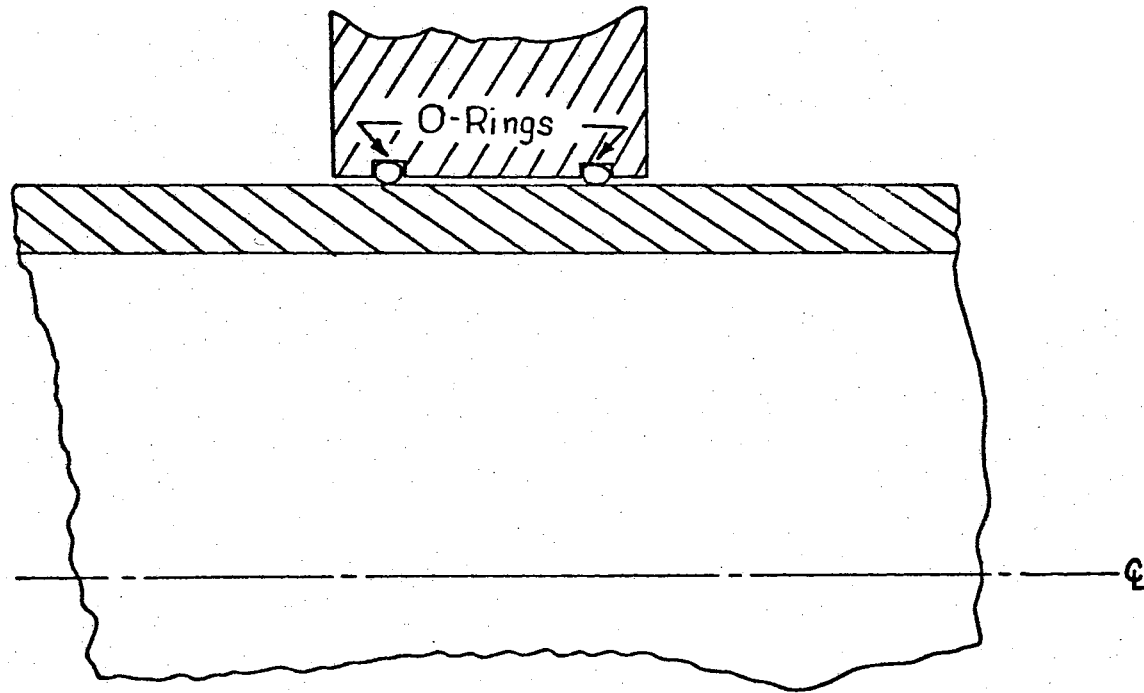
Figure 7. O-Ring Detail.
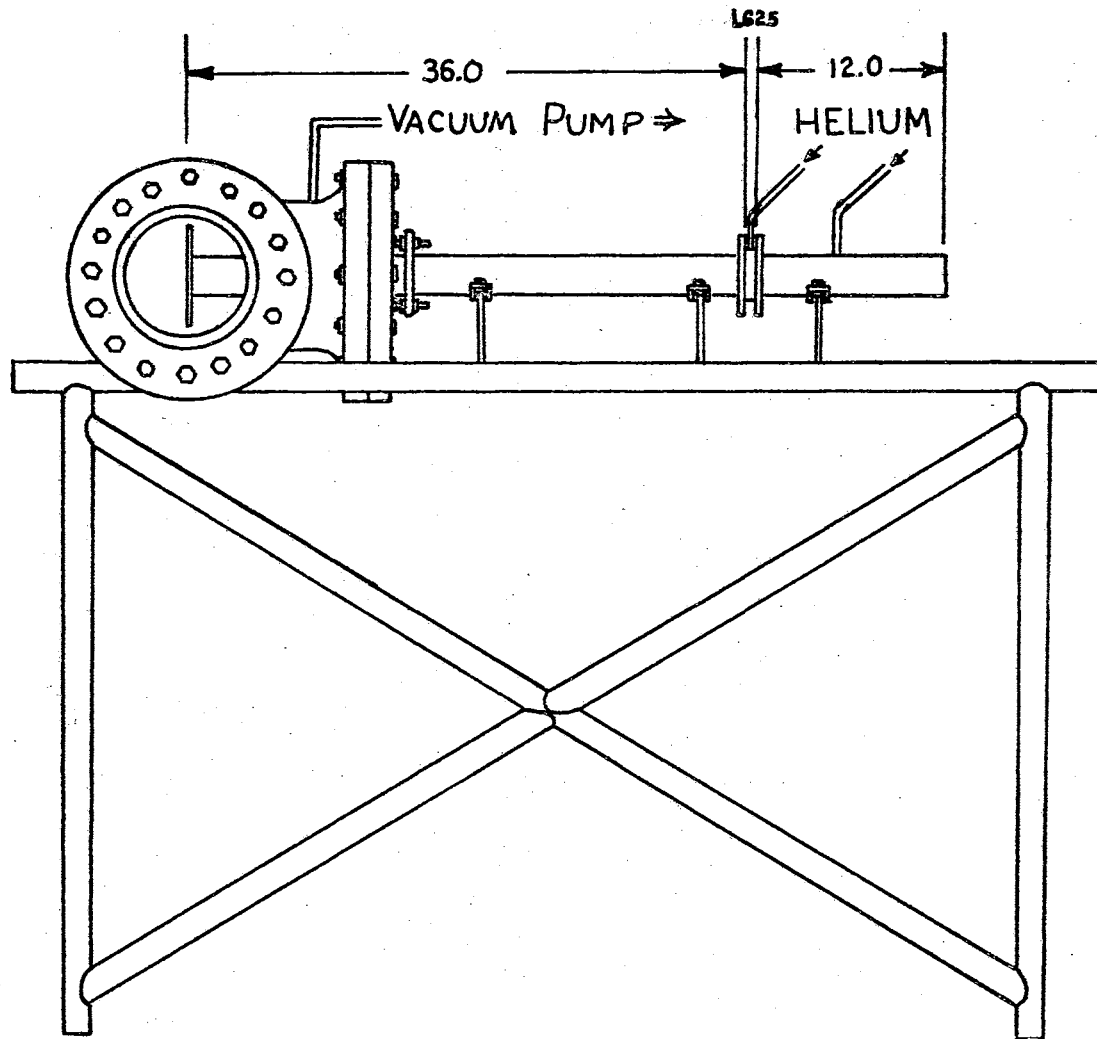
Figure 8. Overall Sketch.

CHAPTER III

INSTRUMENTATION

Shock Velocity

To measure actual shock velocities accurately for comparison with
theoretically calculated values, a pair of recessed Kistler 701 piezo-
electric pressure transducers were mounted a known distance apart, as
shown in Figure 9. The distance varied from six to twenty-four inches.
The rise time of these particular transducers is given by the manufacturers
as 0.3 micro-seconds. For the size transducer used and the shock ve-
locities obtained, the approximate rise time of the signal was estimated
to be from 0.2 to 0.8 micro-seconds. A Beckman/Berkley seven-decade
timing unit was used to record the time of passage of the shock wave
between the two pressure transducers. The counter counted in one micro-
second bits. Sensititivity of the gages and the counter were adjusted
so that the pulse which proceeded down the steel of the tube was of insuf-
ficient strength to initiate counting.

The experimental error in establishing the average velocity of the
shock wave between the gages was estimated to be of the order of + three
per cent. However, the velocity of a shock traveling down a closed tube
is a constantly diminishing value. The placing and selection of the
pressure transducers are trade-offs with experimental error. Ideally,
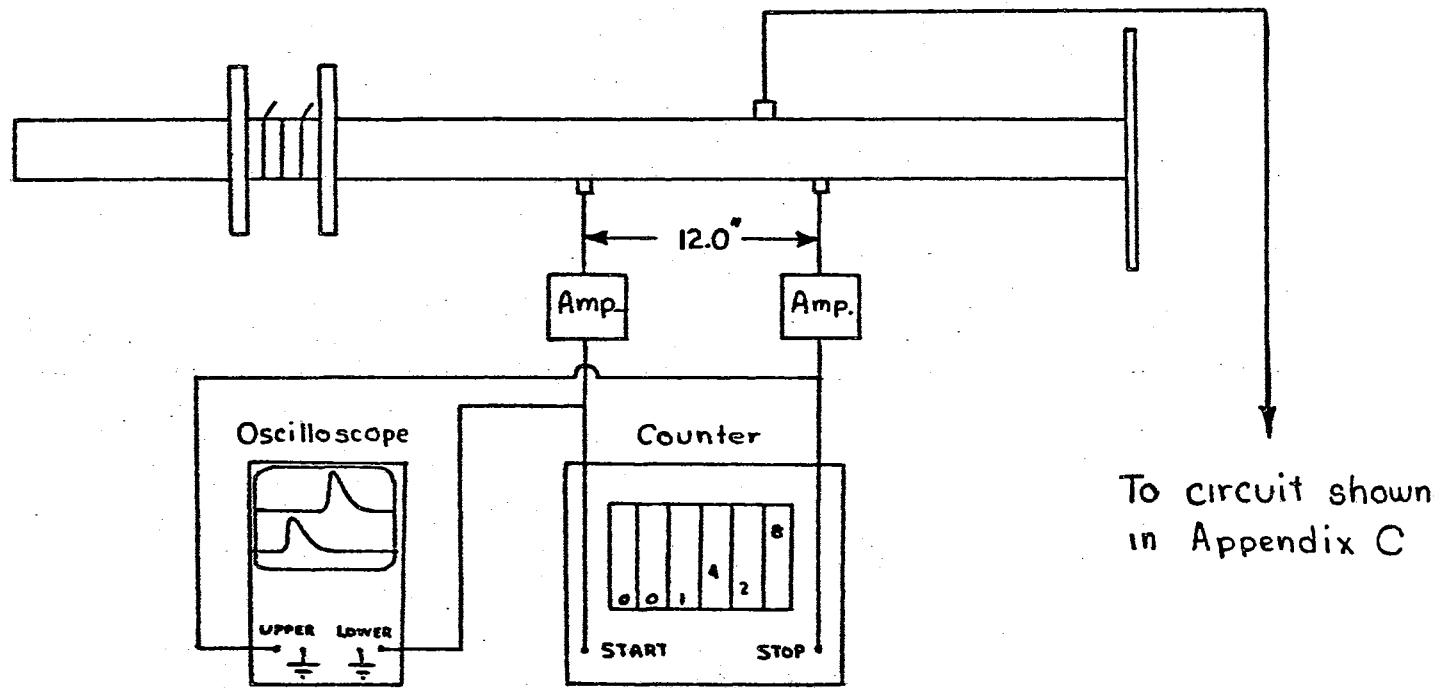
Figure 9. Instrumentation Diagram.

12.0"

Amp.

Amp.

Oscilloscope

Counter

UPPER   LOWER

START   STOP

To circuit shown
in Appendix C

the two gages should be very close together and very near the end of the tube to record a near-instantaneous value of the shock velocity just prior to its emergence into the test area. But, the closer the pressure transducers are located to each other, the greater the per cent of experimental error. Assembly difficulties prevented the placing of the transducers very near the end of the tube. The locations were chosen primarily for convenience of construction.

Shock Pressure Profile

A dual beam Tektronix 535A oscilloscope was placed in the circuit containing the Kistler pressure transducers, as shown in Figure 9. The oscilloscope was adjusted to record the pressure rise of the shock wave as it passed the pressure transducers. A polaroid photograph of the trace produced by the oscilloscope was taken to record the shock pressure profile. A sample photograph may be found in Plate V of the results of this paper. The pressure gages had a natural frequency of 100 kilocycles per second. Experiments showed that the frequency and overtones of the impinging signals produced overshoot and ringing in the transducer response.

Pressure

Driver section pressure was measured on a Marsh one thousand psi gage with an accuracy of $\pm$ 2.5 psi. The pressure in the intermediate section was recorded on an Ashcroft three hundred psi gage with an accuracy of $\pm$ 2.0 psi. The pressures in the receiver assembly and the driven section were measured with a Sun combination positive and

negative pressure gage with an accuracy of $\pm$ 0.05 psi. A schematic of
the pressure instrumentation may be found in Figure 10.

Optical Equipment

An attempt was made to utilize a camera with an electronic shutter,
made by Abtronics. This unit consisted of four light sensitive cells
which were used to create an image on a phosphor screen. This image was
then photographed on a four by five inch plate film. Self contained
timing units permitted the variation of both exposure time and time
interval between exposures. A separate trigger unit was used to actuate
the camera. It was with this trigger that trouble arose. All attempts
to utilize this trigger unit met with failure. For this reason the use
of the above unit was dropped from consideration.

After the failure of the Abtronics camera, an alternate method uti-
lizing a multiple spark source originally designed by Cornell Aeronautical
Laboratory was undertaken. This unit was constructed for future studies
and combined with the existing schlieren system to provide a means of
recording shock behavior. A discussion of the unit is found in Appendix
C. An overall view of the system is found in Figure 11.

Distance-Time Location of Shock

In addition to the multiple spark unit described in Appendix C, the
following method of analysis was devised. Enough test data were taken
to insure the applicability of the method to the facility described in
this work.
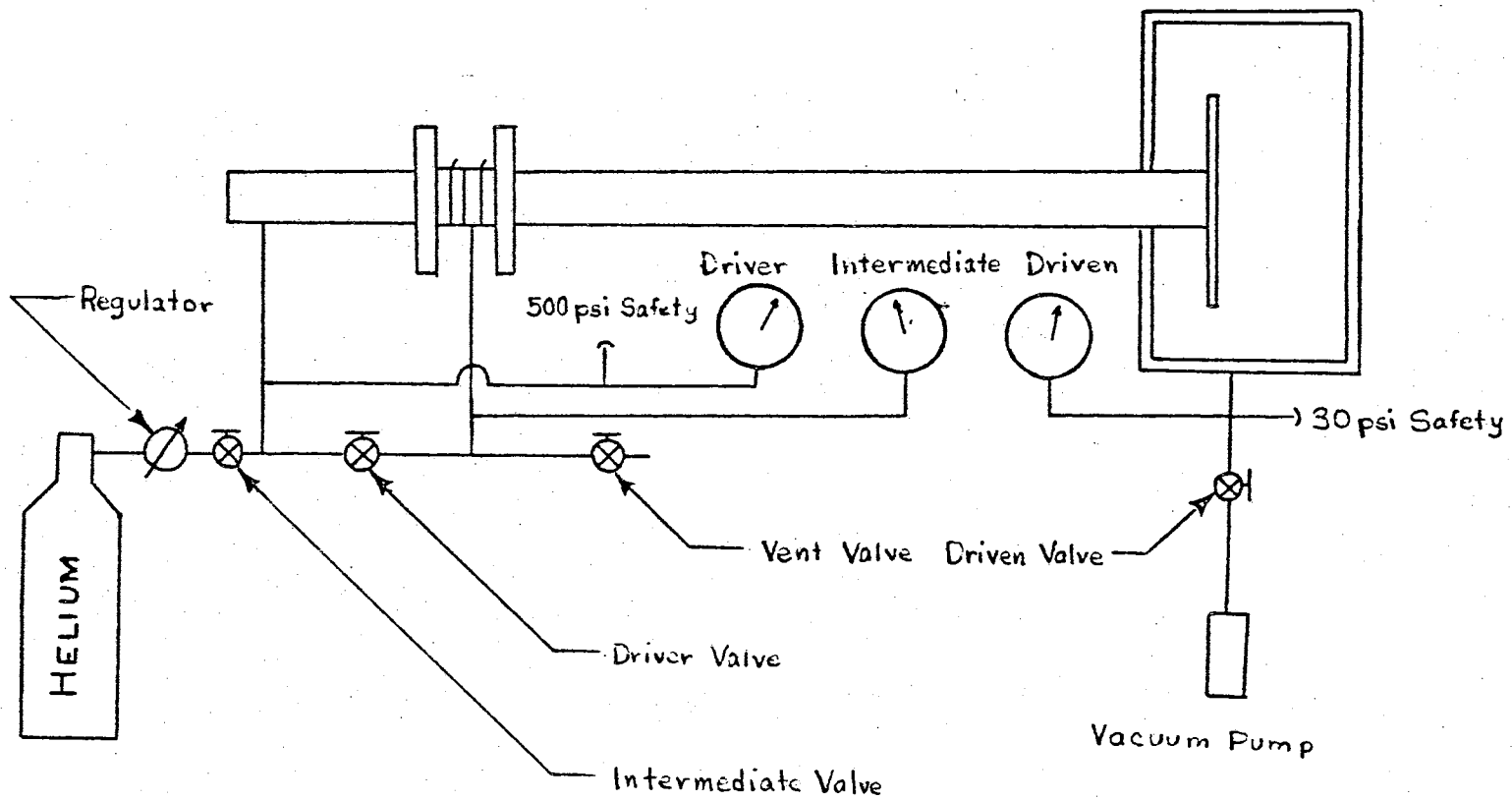
Figure 10. Pressure Schematic.
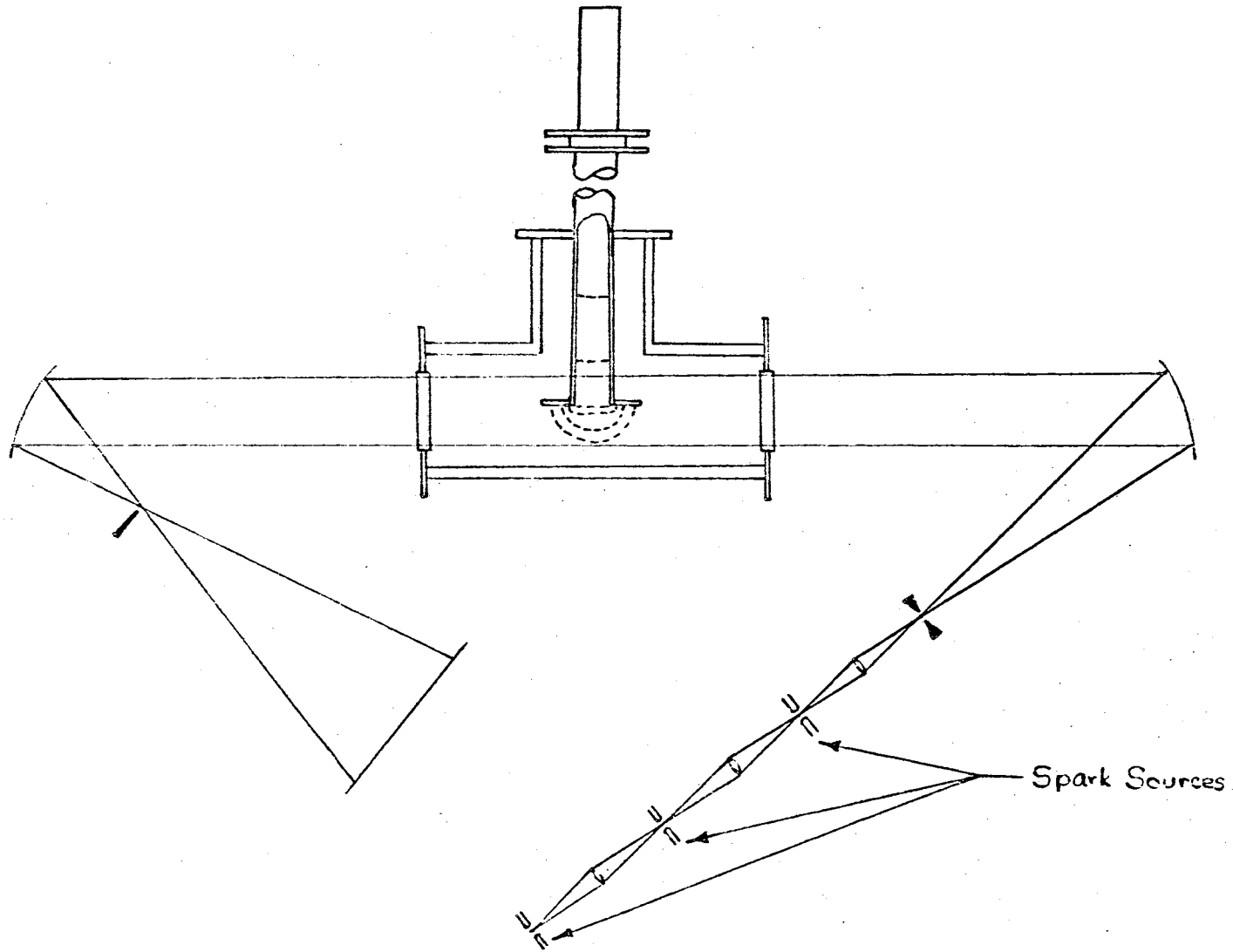
Figure 11. Schlieren Diagram.

Spark Sources

Basically the method consisted of placing pressure transducers at known locations and measuring the time for the expanding wave to travel known distances. The following sketch shows a typical run set-up.
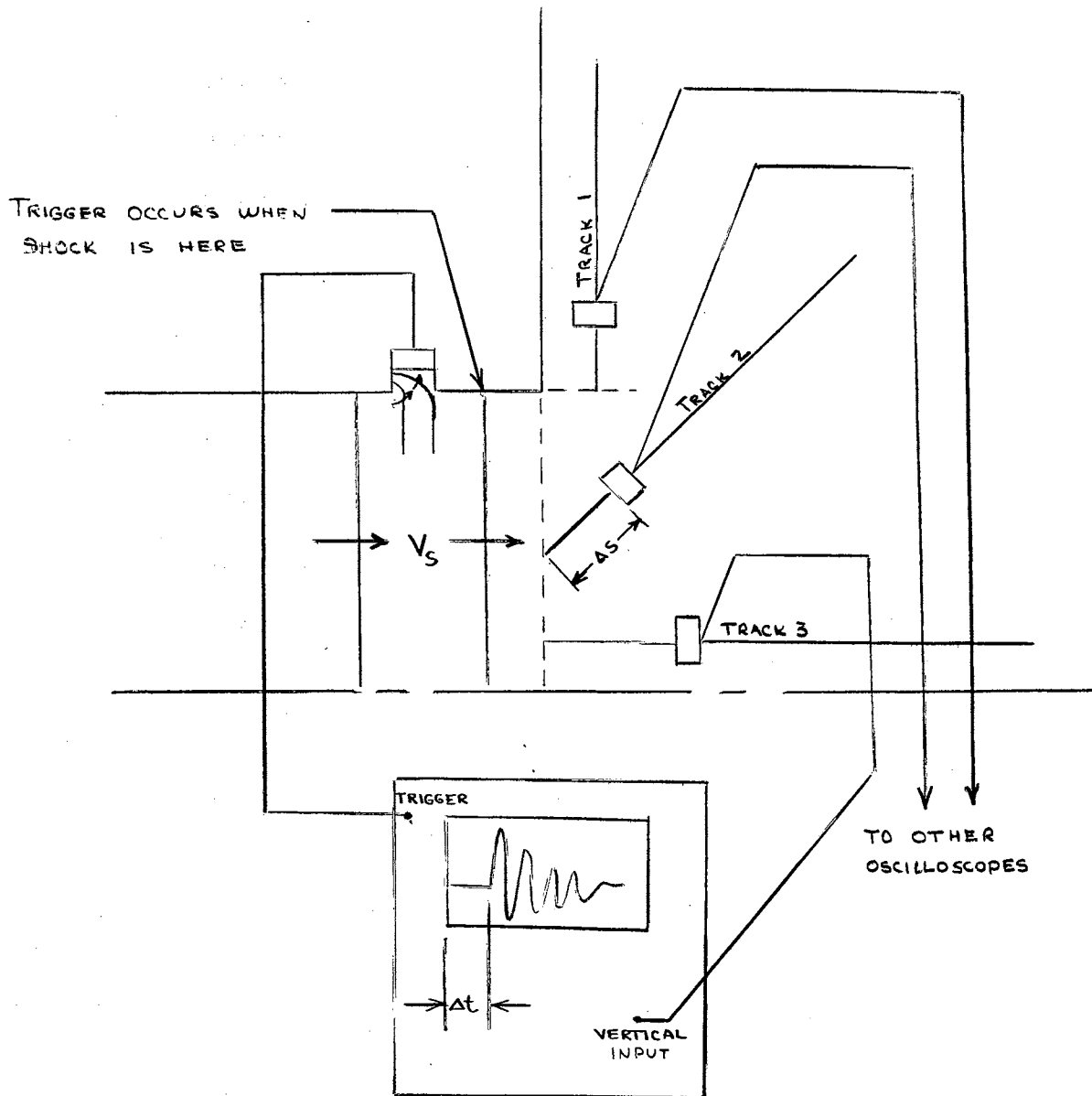
Figure 12. Time-Distance Location Method.

Using the time-distance data gathered for several different tracks, curves similar to the following may be made.
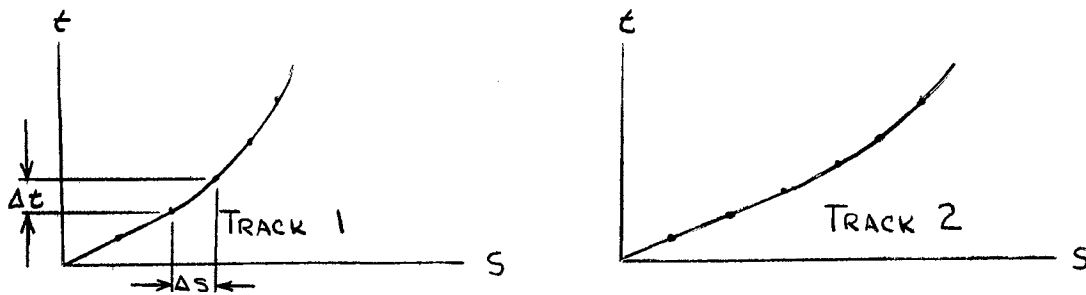
Figure 12a. Time-Distance Plot of Shock Location.

From these plots, a plot of shock location may be made as follows:
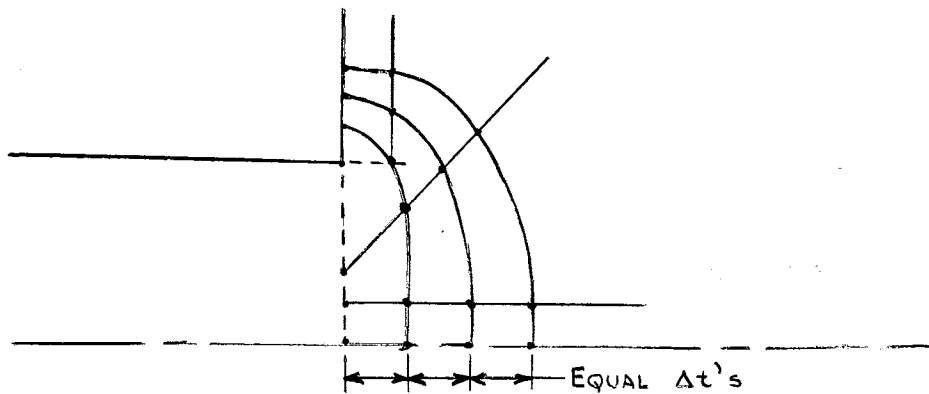
Figure 12b. Shock Location Plot.

Tangents to the shock are then drawn and the perpendicular distance between the tangents is used in the following relation

$v \equiv$ velocity of shock

$\Delta s' \equiv$ distance between shock locations

$\Delta t' \equiv$ time between shock locations

$$v = \frac{\Delta s'}{\Delta t'}$$

CHAPTER IV

SAFETY MEASURES

Construction

Before the system was pressurized with helium it was first hydro-
statically tested at 800 pounds per square inch (double working pressure)
for five minutes in two separate test periods. No leaks of any nature
were found.

Operations

To prevent accidental over-pressurization of the driver section a
500 psi relief valve was installed between the helium bottle and the
driver section. A thirty psi relief valve was installed on the receiver
assembly to prevent accidental over-pressurization of the receiver
section and the resulting blow out of the glass viewing ports.

During operations, the operator of the tube assumed a position such
that the receiver section and the control panel were between him and
the driven section. The plate glass viewing ports were so located that
a catastrophic failure of them would not harm the operator when in the
operating position.

To further protect unrelated personnel within the Mechanical Engi-
neering Laboratory where the tests were conducted, all tests with

pressures in excess of 300 pounds per square inch were run at night
or when the premises were sparsely occupied.

CHAPTER V

TEST TECHNIQUES

Shock Tube Operations

The following steps are to be taken each time the unit is operated.

(1) Place diaphragms in diaphragm holders

(2) Torque bolts to 200 foot-pounds

(3) Make visual check for possible leak sources

(4) Start vacuum pump and switch into tee

(5) Check leakage rate by switching pump in and out

(6) Close helium regulator and open helium bottle valve

(7) Close relief valve and open driver and intermediate valves

(8) Turn helium regulator valve and bring both driver and
     intermediate sections to desired pressure

(9) Close intermediate valve

either

(10) Raise driver pressure to desired valve

(11) Open relief valve slightly; diaphragms will then break

or

(10) Raise driver pressure until diaphragms break

(11) Immediately close driver valve

(12) Close helium bottle valve

(13) Close helium bottle valve

(14) Open intermediate and driver valves

(15) Relieve helium regulator

Instrumentation Operation

To operate the multiple spark source unit it is necessary to perform the following steps.

(1) Turn on low voltage heater supply current

(2) Turn on multi-vibrator voltage supply

(3) Turn on amplifier of 535A oscilloscope and connect to triggering transducer

(4) Charge 0.25 micro-farad capacitors to 10,000 volts with 10KV-5MV power supply

(5) Initiate shock tube operation

(6) Turn off all power supplies

To operate the distance-time location unit the following steps are taken.

(1) Position units at desired location

(2) Attach triggering transducer to trigger of 535A and 551 tektronix oscilloscopes

(3) Mount polaroid cameras on oscilloscopes

(4) Initiate shock tube operation

(5) Use data reduction scheme given in Chapter III

CHAPTER VI

EQUIPMENT

PLATE I
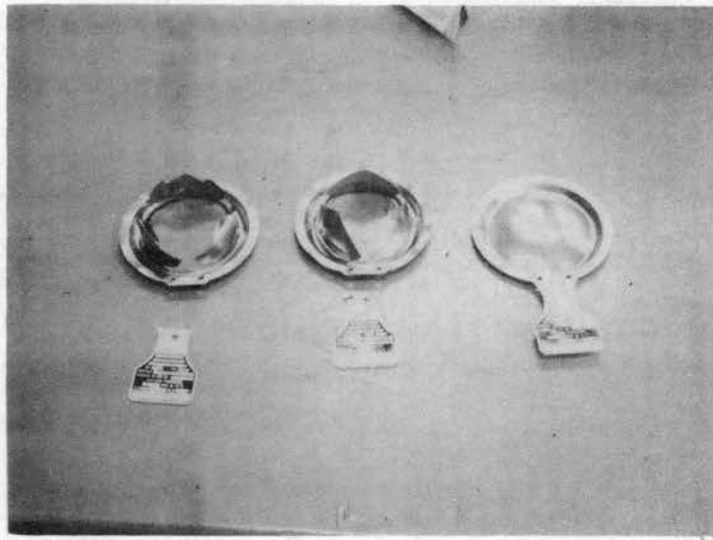
Diaphragms Before and After Breaking
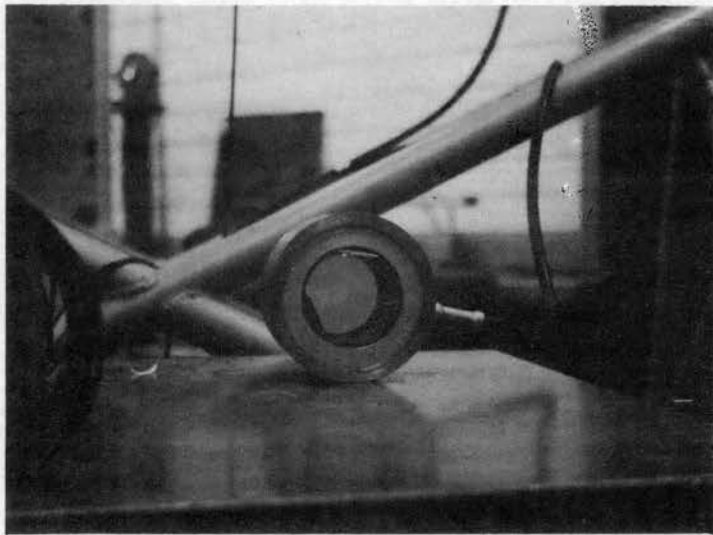
Diaphragm Holders

DIAPHRAGMS AND HOLDERS

PLATE II
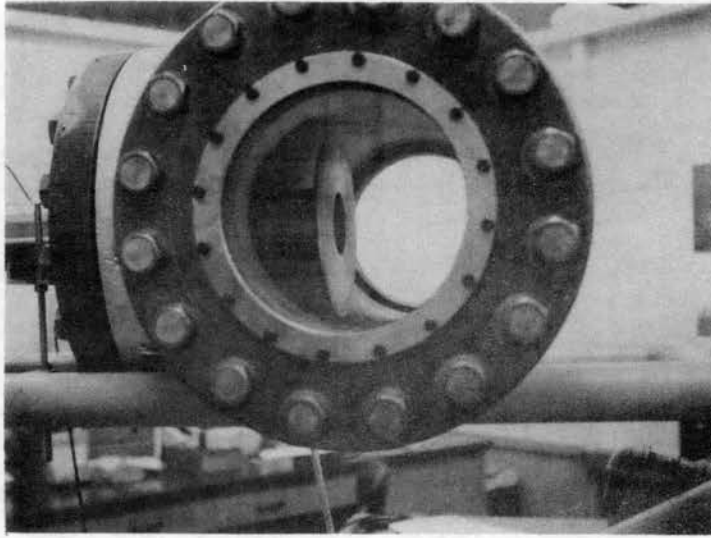
Tee and End Plate
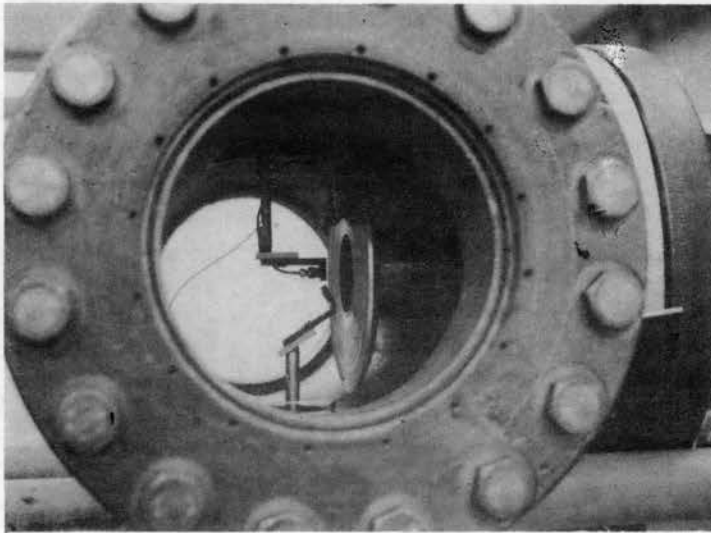
Time-Distance Location Equipment

TEE AND END PLATE WITH TIME-DISTANCE LOCATION EQUIPMENT

PLATE III
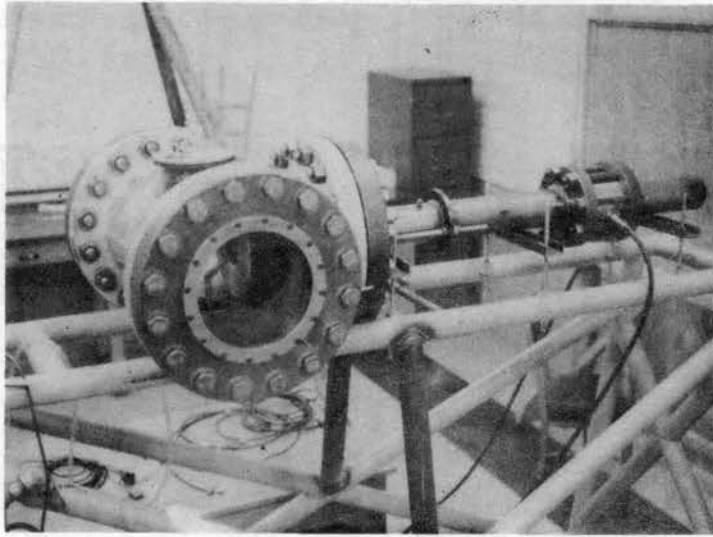
Overall View
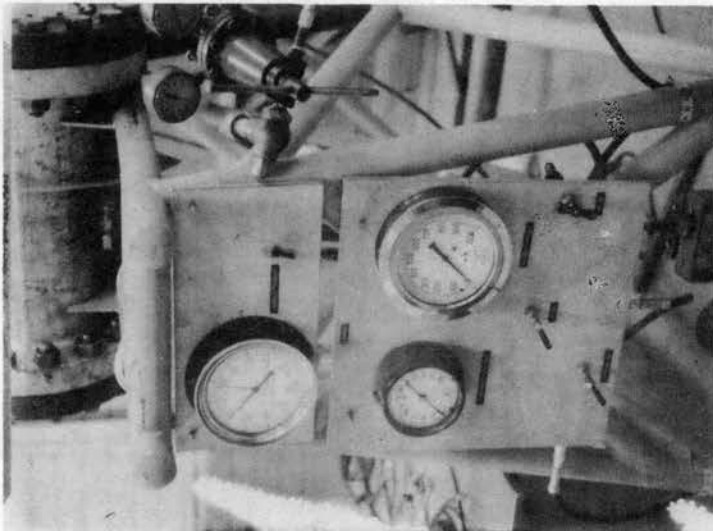
Instrument Panel

OVERALL VIEWS

PLATE IV
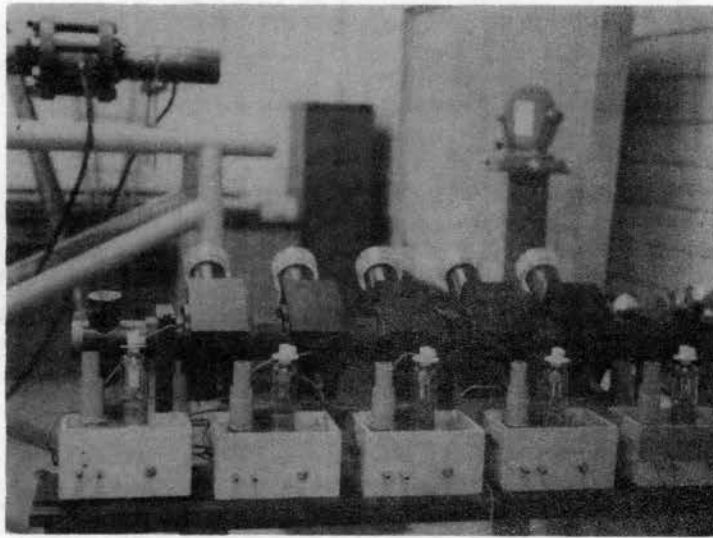
Time Delay Units
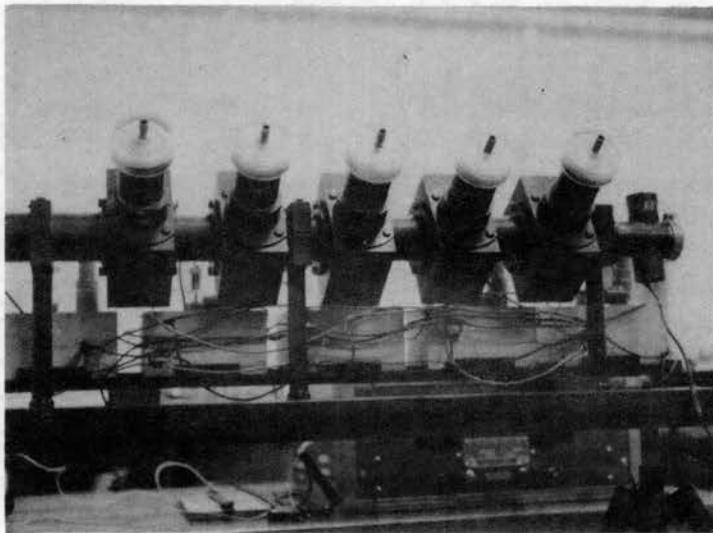
Capacitor Units

MULTIPLE SPARK SOURCE

CHAPTER VII

RESULTS

The following tabular values were obtained from the IBM 1620 computer program described in Appendix B, and from the technique for reflected shocks found in Appendix A. Plotted in Figure 13a are the theoretical values of P_4/P_1 versus Mach number of the shock for conventional single diaphragm theory. Figure 13b gives a comparison between experimental data points and the reflected shock theory described in Appendix A.

TABLE I

SINGLE DIAPHRAGM HELIUM TO AIR-THEORY

γ_1	γ_4	T_1	T_4	M_1	M_4
1.404	1.667	530°R	530°R	28.95	4.003

Mach Number	P_4/P_1
1.00	1.000
1.04	1.137
1.08	1.285
1.12	1.446
1.16	1.620
1.20	1.806
1.24	2.007
1.28	2.223
1.32	2.455
1.36	2.702
1.40	2.967
1.44	3.250
1.48	3.552
1.52	3.873
1.56	4.216
1.60	4.580
1.64	4.967
1.68	5.378
1.72	5.814
1.76	6.277
1.80	6.768
1.84	7.287
1.88	7.837
1.92	8.419
1.96	9.035
2.00	9.686
2.04	10.374
2.08	11.100
2.12	11.867
2.16	12.677
2.20	13.531
2.24	14.433
2.28	15.383
2.32	16.385

TABLE I (Continued)

2.36	17.440
2.40	18.553
2.44	19.725
2.48	20.960
2.52	22.259
2.56	23.628
2.60	25.068
2.64	26.584
2.68	28.179
2.72	29.857
2.76	31.622
2.80	33.479
2.84	35.432
2.88	37.486
2.92	39.645
2.96	41.916
3.00	44.303
3.04	46.812
3.08	49.450
3.12	52.223
3.16	55.138
3.20	58.201
3.24	61.421
3.28	64.805
3.32	68.361
3.36	72.099
3.40	76.027
3.44	80.155
3.48	84.494
3.52	89.054
3.56	93.847
3.60	98.884
3.64	104.179
3.68	109.745
3.72	115.595
3.76	121.745
3,80	128.210
3.84	135.007
3.88	142.153
3.92	149.667
3.96	157.569
4.00	165.879
4.04	174.619
4.08	183.812
4.12	193.482
4.16	203.656

TABLE II

SINGLE DIAPHRAGM HEATED HELIUM TO AIR-THEORY

γ_1	γ_4	T_1	T_4	M_1	M_4
1.404	1.667	530°R	730°R	28.95	4.003

Mach Number	P_4/P_1
1.00	1.000
1.04	1.131
1.08	1.271
1.12	1.423
1.16	1.585
1.20	1.759
1.24	1.945
1.28	2.143
1.32	2.355
1.36	2.580
1.40	2.819
1.44	3.073
1.48	3.343
1.52	3.628
1.56	3.931
1.60	4.250
1.64	4.588
1.68	4.945
1.72	5.322
1.76	5.719
1.80	6.137
1.84	6.578
1.88	7.042
1.92	7.530
1.96	8.043
2.00	8.583
2.04	9.150
2.08	9.745
2.12	10.370
2.16	11.025
2.20	11.713
2.24	12.435
2.28	13.191

TABLE II (Continued)

2.32	13.983
2.36	14.813
2.40	15.683
2.44	16.593
2.48	17.546
2.52	18.543
2.56	19.587
2.60	20.678
2.64	21.820
2.68	23.014
2.72	24.262
2.76	25.567
2,80	26.930
2.84	28.355
2.88	29.844
2.92	31.399
2.96	33.024
3.00	34.721
3.04	36.492
3.08	38.343
3.12	40.274
3.16	42.291
3.20	44.396
3.24	46.593
3.28	48.886
3.32	51.280
3.36	53.777
3.40	56.383
3.44	59.103
3.48	61.940
3.52	64.900
3.56	67.989
3.60	71.211
3.64	74.571
3.68	78.078
3.72	81.736
3.76	85.551
3.80	89.531
3.84	93.683
3.88	98.014
3.92	102.530
3.96	107.243
4.00	112.158
4.04	117.285
4.08	122.633
4.12	128.212
4.16	134.032
4.20	140.103

TABLE II (Continued)

4.24	146.437
4.28	153.044
4.32	159.938
4.36	167.131
4.40	174.635
4.44	182.465
4.48	190.635
4.52	199.161

TABLE III

SINGLE DIAPHRAGM AIR TO AIR-THEORY

γ_1	γ_4	T_1	T_4	M_1	M_4
1.404	1.404	530°R	530°R	28.95	28.95

Mach Number	P_4/P_1
1.00	1.000
1.05	1.256
1.10	1.562
1.15	1.026
1.20	2.356
1.25	2.862
1.30	3.457
1.35	4.154
1.40	4.968
1.45	5.917
1.50	7.021
1.55	8.302
1.60	9.789
1.65	11.512
1.70	13.505
1.75	15.809
1.80	18.472
1.85	21.547
1.90	25.095
1.95	29.190
2.00	33.914
2.05	39.363
2.10	45.649
2.15	52.900
2.20	61.266
2.25	70.921
2.30	82.069
2.35	94.944
2.40	109.823
2.45	127.028
2.50	146.935
2.55	169.986
2.60	196.699
2.65	227.683

TABLE IV

SINGLE DIAPHRAGM HEATED AIR TO AIR-THEORY

Y_1	Y_4	T_1	T_4	M_1	M_4
1.404	1.404	530°R	730°R	28.95	28.95

Mach Number	P_4/P_1
1.00	1.000
1.05	1.235
1.10	1.510
1.15	1.830
1.20	2.202
1.25	2.633
1.30	3.128
1.35	3.698
1.40	4.351
1.45	5.098
1.50	5.950
1.55	6.921
1.60	8.026
1.65	9.281
1.70	10.705
1.75	12.320
1.80	14.148
1.85	16.216
1.90	18.555
1.95	21.198
2.00	24.183
2.05	27.553
2.10	31.357
2.15	35.648
2.20	40.489
2.25	45.949
2.30	52.107
2.35	59.052
2.40	66.885
2.45	75.720
2.50	85.688
2.55	96.936

TABLE IV (Continued)

2.60	109.632
2.65	123.965
2.70	140.154
2.75	158.447
2.80	179.125
2.85	202.512
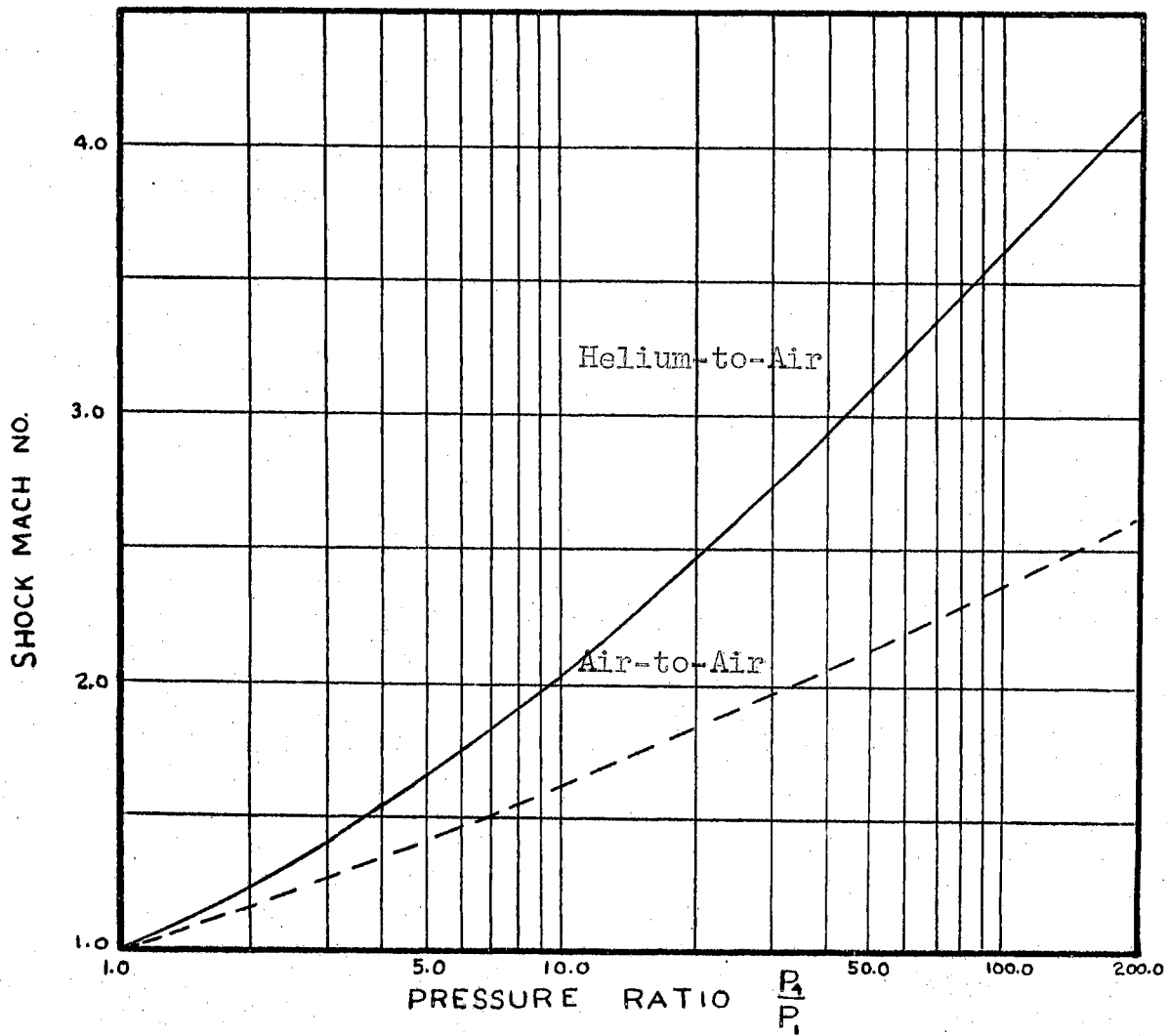
Figure 13a. Single Diaphragm Theory Plots.
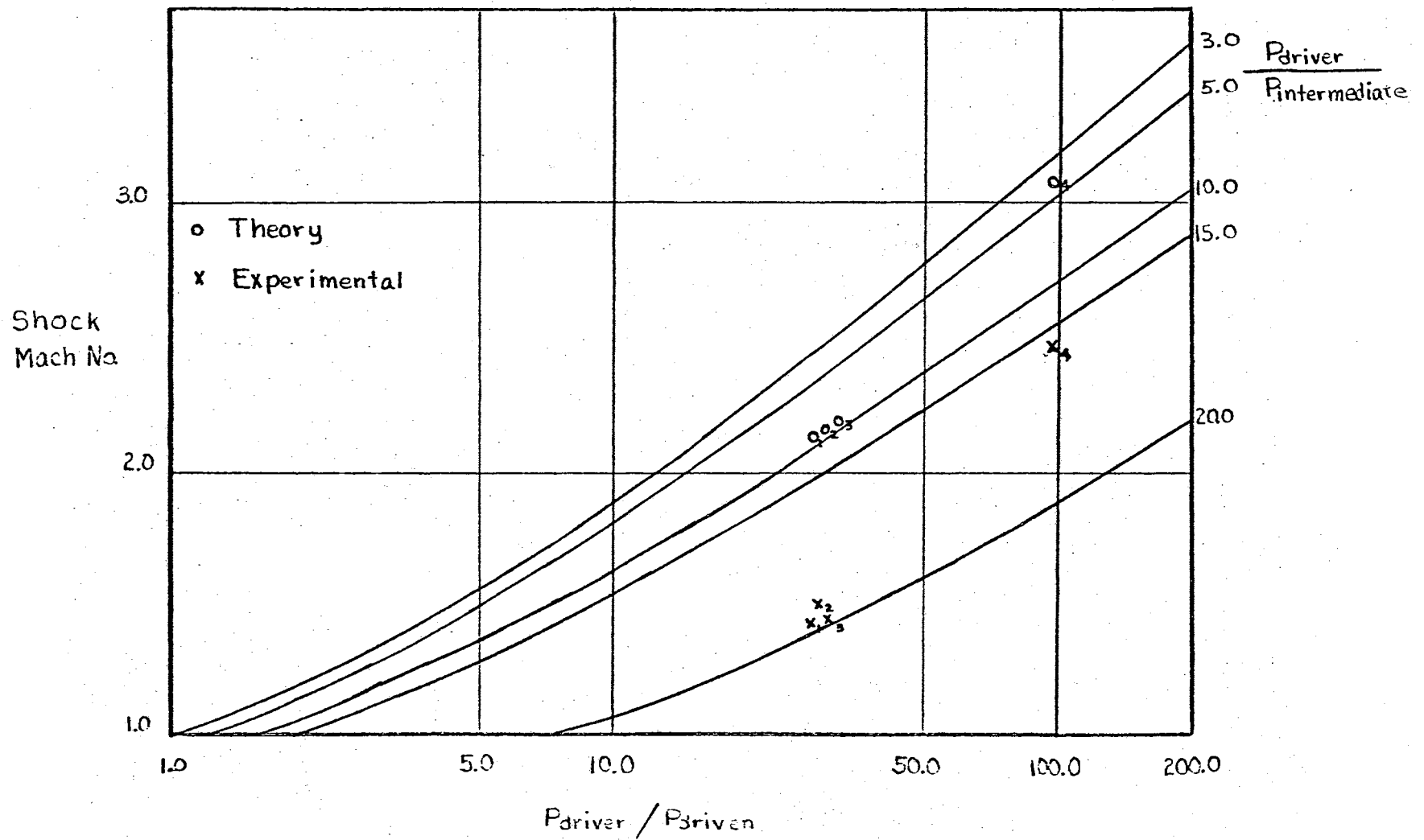
Figure 13b.   Double Diaphragm Theory Plots with Experimental Data Points.

Reflected Shock Stagnation Values

Using a single diaphragm theory for a Helium-Helium shock tube, it is found that the following points exist for the shock wave resulting from the upstream diaphragm bursting.

Mach No. (M)	Pressure Ratio $(P_4/P_{intermediate})$
1.222	3.0
1.369	5.0
1.558	10.0
1.662	15.0
1.743	20.0

These pressure ratios are then used in the technique given by Shapiro (9)(see Appendix A, Section 3) to find the pressures and temperatures existing behind a reflected shock. The technique yields the following, remembering that P_{driver} and $P_{intermediate}$ are related to the critical pressure.

Mach No.	$P_{intermediate}$	P_4	T(after reflection)	P_4, (after reflection)
1.222	130 psia	390 psia	819°R	373 psia
1.369	65 psia	325 psia	906°R	258 psia
1.558	28.8 psia	288.8 psia	1192°R	185 psia
1.662	18.6 psia	278.6 psia	1311°R	147 psia
1.743	3.6 psia	263.6 psia	1438°R	34.2 psia

Using these values as stagnation values for the second diaphragm and correlating the pressure ratios obtained to P_{driver} (P_4), Table V

results. The values obtained are plotted in Figure 13b.

$$\frac{P_4}{P_1} = \frac{P_4{}'}{P_1} \frac{P_1}{P_4{}'}$$

$\dfrac{P_4{}'}{P_1}$ obtained from program; $\dfrac{P_4}{P_4{}'}$ obtained above.

TABLE V

DOUBLE DIAPHRAGM - REFLECTED SHOCK - HELIUM TO AIR-THEORY

γ_1	$\gamma_{intermediate}$	γ_4	$T_1 = T_4 = T_{intermediate}$ (initially)
1.404	1.667	1.667	530.0°R

Mach Number	P_4/P_1	$P_4/P_{intermediate}$
1.00	1.045	3.0
1.10	1.458	3.0
1.20	1.970	3.0
1.30	2.605	3.0
1.40	3.380	3.0
1.50	4.310	3.0
1.60	5.420	3.0
1.70	6.760	3.0
1.80	8.330	3.0
1.90	10.120	3.0
2.00	12.460	3.0
2.10	15.050	3.0
2.20	18.100	3.0
2.30	21.650	3.0
2.40	25.830	3.0
2.50	30.800	3.0
2.60	36.600	3.0
2.70	43.200	3.0
2.80	51.100	3.0
2.90	60.400	3.0
3.00	70.000	3.0
3.10	83.500	3.0
3.20	98.200	3.0
3.30	115.200	3.0
3.40	135.300	3.0
3.50	154.000	3.0
3.60	186.500	3.0
1.00	1.211	5.0
1.10	1.700	5.0
1.20	2.310	5.0

TABLE V (Continued)

1.30	3.080	5.0
1.40	4.020	5.0
1.50	5.140	5.0
1.60	6.500	5.0
1.70	8.150	5.0
1.80	10.110	5.0
1.90	12.430	5.0
2.00	15.220	5.0
2.10	18.540	5.0
2.20	22.450	5.0
2.30	27.000	5.0
2.40	32.500	5.0
2.50	38.900	5.0
2.60	45.400	5.0
2.70	55.400	5.0
2.80	65.900	5.0
2.90	78.400	5.0
3.00	92.900	5.0
3.10	110.000	5.0
3.20	130.500	5.0
3.30	154.500	5.0
3.40	182.500	5.0
3.50	216.500	5.0
1.00	1.563	10.0
1.10	2.235	10.0
1.20	3.095	10.0
1.30	4.170	10.0
1.40	5.540	10.0
1.50	7.220	10.0
1.60	9.300	10.0
1.70	11810	10.0
1.80	14.930	10.0
1.90	18.720	10.0
2.00	23.300	10.0
2.10	28.900	10.0
2.20	35.600	10.0
2.30	43.800	10.0
2.40	53.600	10.0
2.50	65.500	10.0
2.60	80.000	10.0
2.70	97.300	10.0
2.80	118.100	10.0
2.90	143.300	10.0
3.00	174.100	10.0
3.10	212.000	10.0

TABLE V (Continued)

1.00	1.896	15.0
1.10	2.725	15.0
1.20	3.800	15.0
1.30	5.170	15.0
1.40	6.880	15.0
1.50	9.050	15.0
1.60	11.710	15.0
1.70	15.030	15.0
1.80	19.080	15.0
1.90	24.100	15.0
2.00	30.020	15.0
2.10	37.700	15.0
2.20	46.900	15.0
2.30	58.000	15.0
2.40	71.500	15.0
2.50	88.000	15.0
2.60	108.200	15.0
2.70	133.000	15.0
2.80	163.100	15.0
2.90	200.000	15.0
1.00	7.700	20.0
1.10	11.120	20.0
1.20	15.620	20.0
1.30	21.400	20.0
1.40	28.700	20.0
1.50	38.000	20.0
1.60	49.500	20.0
1.70	64.000	20.0
1.80	81.800	20.0
1.90	104.000	20.0
2.00	131.200	20.0
2.10	165.200	20.0
2.20	206.000	20.0

Sample Calculation of Time-Distance Method

Using the values given below, which were obtained experimentally, it is possible to plot the location of the emerging shock front.

Experimental Data

| Run | Track 1 | | Track 2 | | Track 3 | |
	Time(t)	Distance(S)	Time(t)	Distance(S)	Time(t)	Distance(S)
1	23	0.385	--	--	--	--
2	32	0.562	26	0.484	20	0.219
3	41	0.750	27	0.484+	22	0.250

The distances given are measured from the plane of the shock tube exit to the transducer along each track.

$$V_{average} = \left(\frac{{}_1S_2}{{}_1t_2} + \frac{{}_1S_3}{{}_1t_3} \right) /2 = 1665 \text{ ft/sec}$$

Since there is a delay between the time the shock passes the trigger transducer and the time the oscilloscope sweep or counting unit initiates action, the following correction is made.

$$S' = \text{actual distance traveled} = V_{average} \; {}_0t_1 = 0.420 \text{ inches}$$

Therefore, at time zero the shock is still (S'-S) inches inside the tube.

$$S' - S = 0.035 \text{ inches}$$

The time correction to be subtracted from all experimental time values is:

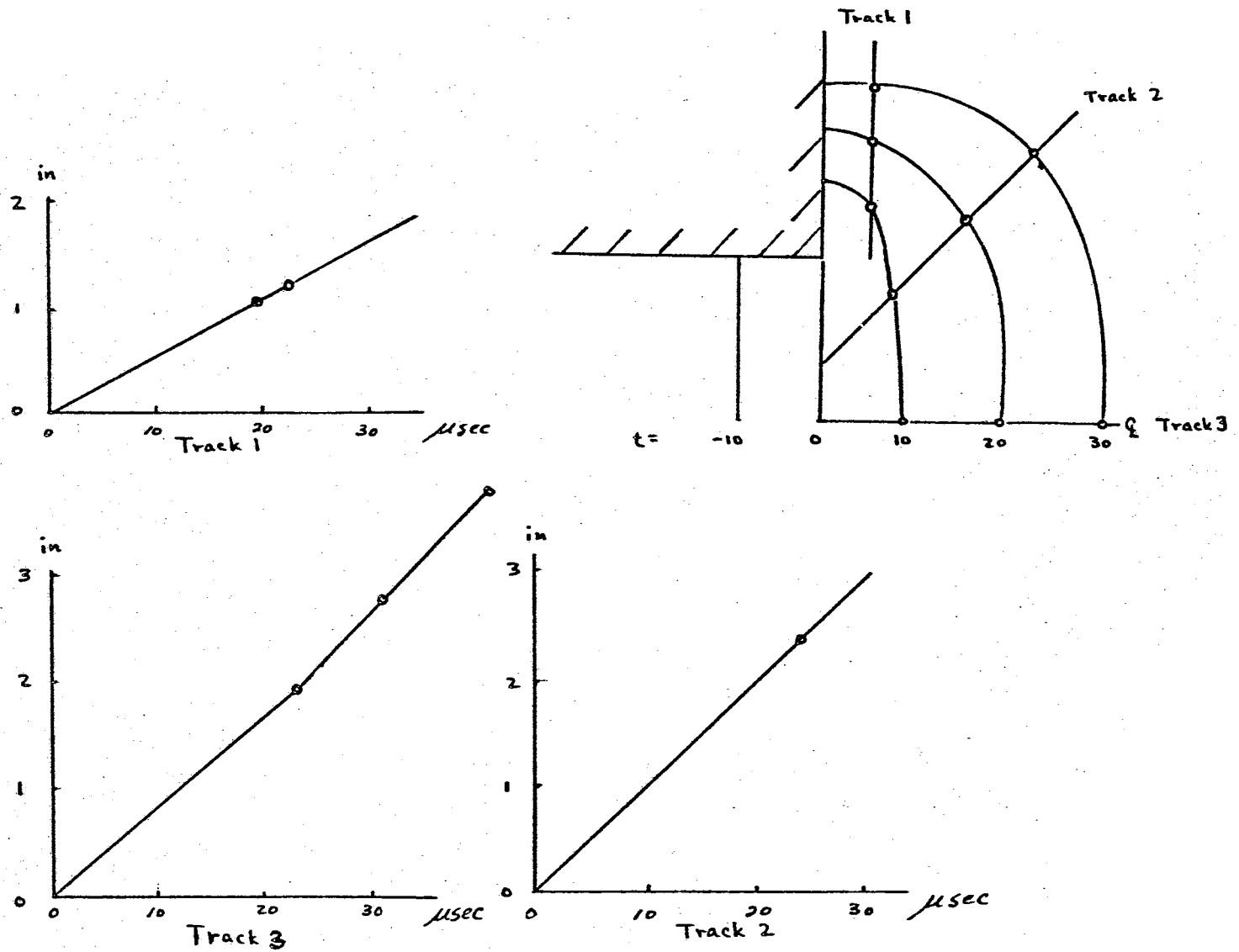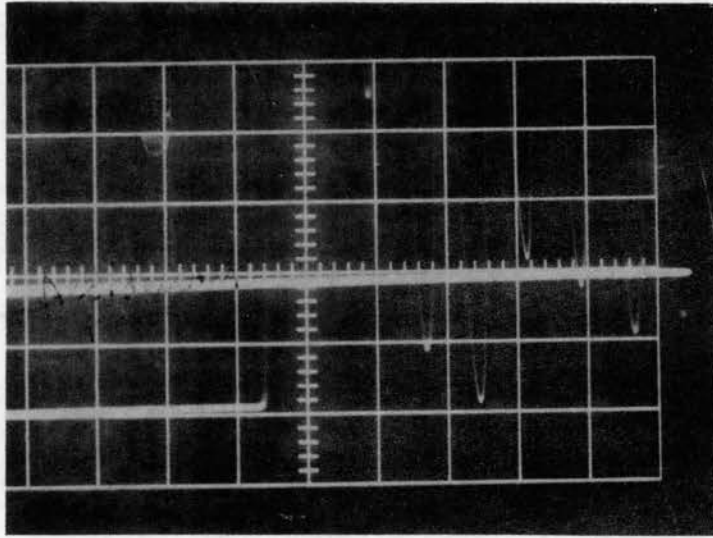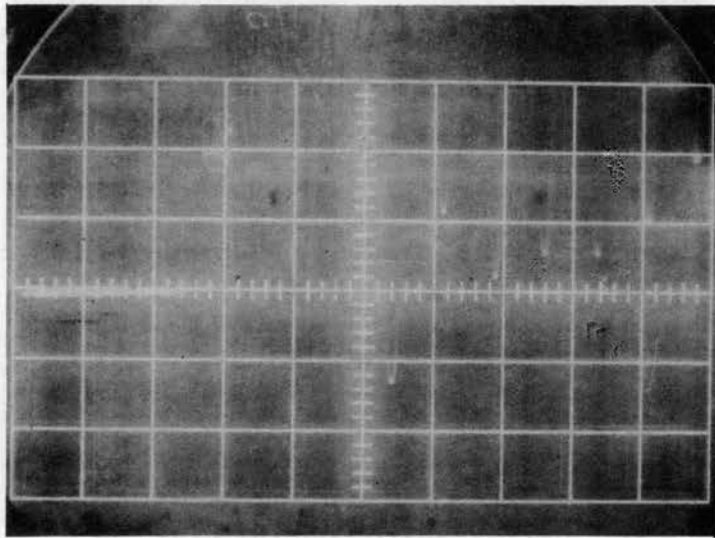$$t' = \frac{S'-S}{V_{average}} = 1.75 \text{ micro-seconds}$$

Figure 14. Experimental Time-Distance Plots.

PLATE V

Pressure Profile showing Ringing of Kistler
Pressure Transducer

Typical Trace for Obtaining Shock Location
With Head-on Impact

OSCILLOSCOPE TRACES

CHAPTER VIII

CONCLUSIONS AND RECOMMENDATIONS

As expected, the experimental values of the Mach number were somewhat lower than the theoretical values calculated by the reflected shock technique. This discrepancy may be caused by energy expended in breaking the diaphragms and by imperfect diaphragm opening. Experimental data indicate that the difference between theoretical and experimental values decreases slightly as the driver pressure increases. This result was expected because the energy losses of the tube previously mentioned are not a particularly strong function of pressure ratio and remain essentially constant. Therefore, the percentage loss in shock strength decreases as the total possible shock strength increases.

It is therefore concluded that the shock tube facility described in this paper should follow the results predicted by a reflected shock analysis with certain losses as explained in Chapter II.

Difficulty was experienced in obtaining consistent triggering of measuring devices. It is recommended that the recessed Kistler gages be replaced with flush-mounted gages. This will eliminate much of the uncertainty of the present triggering method.

If higher shock Mach numbers are desired, it is recommended that the Sun vacuum gage be replaced with a gage of better accuracy. By reducing the experimental error in reading the gage to 0.01 pounds per

60

square inch, it is possible to operate the facility at an overall

pressure ratio of 1000:1 with the same accuracy now available.

It is further recommended that the venting system for the inter-

mediate pressure section be modified to reduce further the surge volume

and flow orifice. This will result in the ability to utilize the shock

tube at lower driver-to-driven ratios while maintaining the driver-to-

intermediate section ratios at high values.

All pressure gages presently in use should be replaced with gages

which provide a permanent record of maximum pressures recorded.

Based on the results presented in this study, the conclusion reached

is that the facility promises to deliver the results desired, subject

to limitations discussed previously.

SELECTED BIBLIOGRAPHY

(1)   Lee, R. C. K., J. R. Ruetenik, and E. A. Wittmer. An Exploratory
      Study of the Generation of Blast-type Profiles in the Shock
      Tube by the Reflection Method. WADC TR 54-383, AD-97323,
      August 1, 1956.

(2)   Rabinowicz, Josef. Aerodynamic Studies in the Shock Tube.
      Guggenheim Aeronautical Laboratory, California Institute
      of Technology, Memorandum No. 38.

(3)   Evans, R. C. Operation and Performance of a Shock Tube with
      Heated Driver. Guggenheim Aeronautical Laboratory,
      California Institute of Technology, Memorandum No. 48.

(4)   Elder, F. K, Jr., and N. de Haas. Schlieren Studies of Initial
      Conditions at the Open End of a Cylindrical Shock Tube.
      The John Hopkins University Applied Physics Laboratory,
      April 29, 1952.

(5)   Lee, J. D. Some Aspects of Flight Through a Nuclear Blast and
      Its Laboratory Simulation. Research Report, SC-RR-64-1781
      Aerodynamics, Sandia Corporation, January, 1965.

(6)   Pierce, D. Simulation of Blast Waves in a Supersonic Wind
      Tunnel. Royal Aircraft Establishment, Technical Note No.
      Aero. 2665, January, 1960.

(7)   Bingham, C. J. and T. E. Davidson. Investigation of Simulation
      of Shock-Shock Interaction in Hypersonic Gasdynamic Test
      Facility. FDL-TDR-64-9, March, 1964.

(8)   Black, Sivalls, and Bryson, Inc. Use of Blow-out Discs. Brochure
      published by manufacturer of diaphragms used in study.

(9)   Shapiro, A. H. The Dynamics and Thermodynamics of Compressible
      Fluid Flow. The Ronald Press Company, New York, 1953.

(10) Liepmann, H. W. and A. Roshko. Elements of Gas Dynamics.
      John Wiley & Sons, Inc., New York, 1957.

(11) Fitzpatrick, Hubbard, and Thaley. Journal of Applied Physics.
      21, 1269, 1950.

APPENDIX A

APPENDIX A

SECTION I

Assuming a centered expansion wave and shock front the following relations may be obtained.

First consider only the shock front. It moves into the ambient gas with velocity V_s, leaving the disturbed gas with velocity U_2.
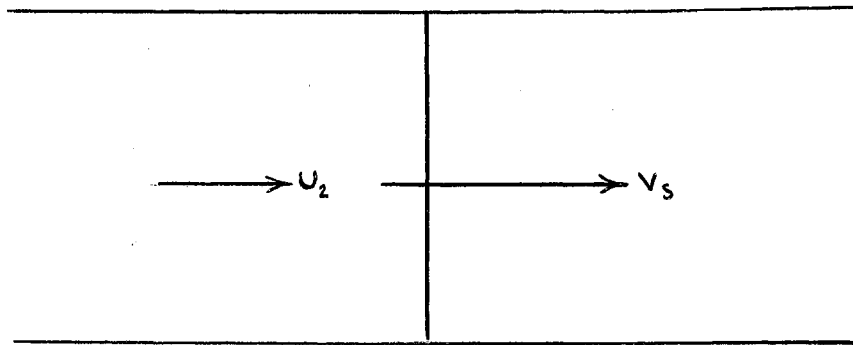

Figure 15. Moving Shock Front.

A transform of the above physical situation may be achieved by causing the gas to flow into a stationary shock wave. This is shown below.
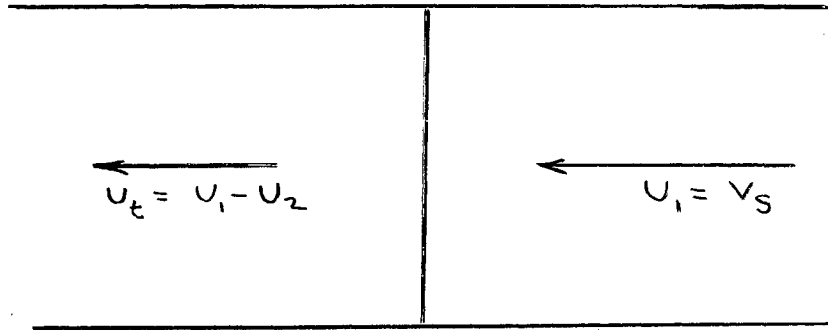
Figure 16. Transformation of Moving Shock Front.

By definition the Mach number of the shock (M_s) is:

$$(1) \qquad M_s \equiv \frac{V_s}{a_{ambient}} = \frac{U_1}{a_1}$$

For a perfect gas the pressure ratio across a shock is

$$(2) \qquad \frac{P_2}{P_1} = 1 + \frac{2\gamma_1}{\gamma_1 + 1}(M_s^2 - 1) \qquad \text{or}$$

$$(3) \qquad M_s = \left[\left(\frac{P_2}{P_1}\right)\left(\frac{\gamma_1 + 1}{2\gamma_1}\right) + 1\right]^{\frac{1}{2}}$$

Substituting (3) into (1) and solving for U_1 gives:

$$(4) \qquad U_1 = a_1\left[\left(\frac{\gamma_1 + 1}{2\gamma_1}\right)\frac{P_2}{P_1} + \frac{\gamma_1 - 1}{2\gamma_1}\right]^{\frac{1}{2}}$$

The Rankine-Hugoniot relation for density is:

$$(5) \qquad \frac{P_2}{P_1} = \frac{1 + \left(\frac{\gamma_1 + 1}{\gamma_1 - 1}\right)\frac{P_2}{P_1}}{\left(\frac{\gamma_1 + 1}{\gamma_1 - 1}\right) + \frac{P_2}{P_1}} = \frac{U_2}{U_1}$$

Now from Figure A-2 $U_t = U_1 - U_2$

Rearranging gives:

$$(6) \qquad U_t = U_1 \left(1 - \frac{U_2}{U_1}\right)$$
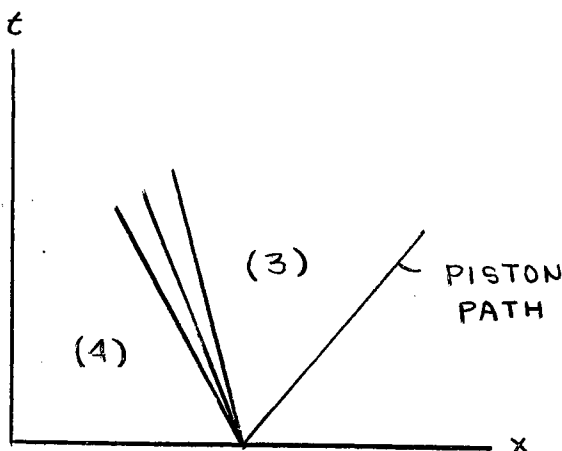
Substituting (4) and (5) into (6) results in

$$U_t = a_1 \left[\frac{\gamma_1+1}{2\gamma_1} \left(\frac{P_2}{P_1}\right) + \frac{\gamma_1-1}{2\gamma_1} \right]^{\frac{1}{2}} \left[1 - \frac{1 + \left(\frac{\gamma_1+1}{\gamma_1-1}\right)\frac{P_2}{P_1}}{\left(\frac{\gamma_1+1}{\gamma_1-1}\right) + \frac{P_2}{P_1}} \right]$$

Simplifying gives:

$$(7) \qquad U_t = \frac{a_1}{\gamma_1} \left(\frac{P_2}{P_1} - 1\right) \left[\frac{\left(\frac{2/\gamma_1}{\gamma_1+1}\right)}{\left(\frac{P_2}{P_1} + \frac{\gamma_1-1}{\gamma_1+1}\right)} \right]^{\frac{1}{2}}$$

Now, considering an expansion wave, the following relations are true. That the expansion is isentropic and rapidly flattens into a gradual rise is shown well by Shapiro (9) and Liepmann and Roshko (10).

For the condition at left, produced by a receding piston, the following relations are given by Liepmann and Roshko (10).

Figure 17.   Expansion Wave.

$$(8) \qquad C_3 = a_4 - \frac{\gamma_4 + 1}{2} U_t$$

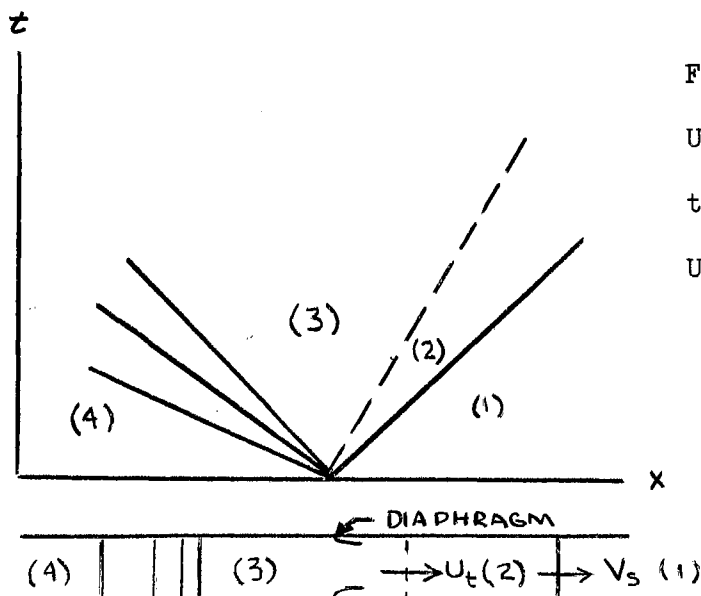$$(9) \qquad U_t = \frac{2}{\gamma_4 - 1} (a_3 - a_4)$$

$$(10) \qquad a_3 = a_4 \left(\frac{\rho_3}{\rho_4} \right)^{\frac{\gamma_4 - 1}{2}}$$

Substituting (10) into (9) and solving for $\frac{\rho_3}{\rho_4}$ gives:

$$\frac{\rho_3}{\rho_4} = \left[1 - \left(\frac{\gamma_4 - 1}{2} \right) \frac{U_t}{a_4} \right]^{\frac{2}{\gamma_4 - 1}} \quad \text{and since} \quad \frac{P_3}{P_4} = \left(\frac{\rho_3}{\rho_4} \right)^{\gamma_4};$$

$$(11) \qquad \frac{P_3}{P_4} = \left[1 - \left(\frac{\gamma_4 - 1}{2} \right) \frac{U_t}{a_4} \right]^{\frac{2\gamma_4}{\gamma_4 - 1}}$$

A time distance plot for a shock tube is as follows:

From continuity considerations $U_2 = U_3$ and $P_2 = P_3$ across the contact surface and $U_2 = U_3 = U_t$.

Figure 18. Time-Distance Plot.

$$(7) \quad U_2 = \frac{a_1}{\gamma_1} \left(\frac{P_2}{P_1} - 1 \right) \left[\frac{\frac{2}{\gamma_1}}{\frac{P_2}{P_1}(\gamma_1+1)+(\gamma_1-1)} \right]^{\frac{1}{2}}$$

Combining (9), (10), and (11) gives:

$$(7a) \quad U_3 = \left(\frac{2a_4}{\gamma_{4}-1} \right) \left[1 - \left(\frac{P_3}{P_4} \right)^{\frac{\gamma_4-1}{2\gamma_4}} \right]$$

Equating the (7) and (7a) gives:

$$\frac{a_1}{\gamma_1} \left(\frac{P_2}{P_1} - 1 \right) \left[\frac{\frac{2}{\gamma_1}}{\frac{P_2}{P_1}(\gamma_1+1)+(\gamma_1-1)} \right]^{\frac{1}{2}} = \left(\frac{2a_4}{\gamma_{4}-1} \right) \left[1 - \left(\frac{P_3}{P_4} \right)^{\frac{\gamma_4-1}{2\gamma_4}} \right]$$

Substituting $P_3 = P_2$ and multiplying by $\left(\frac{P_1}{P_2} \right)^{\frac{\gamma_4-1}{2\gamma_4}}$ results in:

$$\frac{a_1}{\gamma_1} \left[\left(\frac{P_1}{P_2} \right)^{-\frac{\gamma_4-1}{2\gamma_4}} - \left(\frac{P_1}{P_2} \right)^{\frac{\gamma_4-1}{2\gamma_4}} \right] \left[\frac{\frac{2}{\gamma_1}}{\frac{P_2}{P_1}(\gamma_1+1)+(\gamma_1-1)} \right]^{\frac{1}{2}} =$$

$$= \frac{2a_4}{(\gamma_{4}-1)} \left(\frac{P_1}{P_2} \right)^{\frac{\gamma_4-1}{2\gamma_4}} - \left(\frac{2a_4}{(\gamma_{4}-1)} \right) \left(\frac{P_1}{P_4} \right)^{\frac{\gamma_4-1}{2\gamma_4}}$$

Solving for $\frac{P_4}{P_1}$ gives:

$$(12) \quad \frac{P_4}{P_1} = \frac{P_1}{P_2} \left\{ 1 - \frac{\frac{a_1}{a_4} \left[\frac{\gamma_4-1}{(2\gamma_1)}^{\frac{1}{2}} \right] \left(\frac{P_2}{P_1} - 1 \right)}{\gamma_1 + \frac{P_2}{P_1}(\gamma_1+1) - 1} \right\}^{-\frac{2\gamma_4}{\gamma_{4}-1}}$$

Writing (12) in terms of $\dfrac{U_3}{a_1} = \dfrac{U_2}{a_1} = M_s$ where M_s is given by (3) results in:

$$(13) \quad \frac{P_4}{P_1} = \left(\frac{\gamma_1 - 1}{\gamma_1 + 1}\right)\left[\frac{2\gamma_1 M_s^2}{\gamma_1 - 1} - 1\right]\left[1 - \left(\frac{\gamma_4 - 1}{\gamma_1 + 1}\right)\left(\frac{M_s^2 - 1}{\frac{a_4}{a_1} M_s}\right)\right]^{-\frac{2\gamma_4}{\gamma_4 - 1}}$$

The above equation was used to obtain Tables I, II, III, and IV.

Double Diaphragm Configuration

An almost universal concept among beginning users of shock tubes is the belief that a multiple diaphragm arrangement always causes an increase in performance over a single diaphragm arrangement. Data and discussions in most shock tube literature leave the impression that for a given ratio of driver pressure to driven pressure $(P_{4n}/P_1$ for an n-diaphragm shock tube), a higher Mach number for the shock front may be obtained by the use of multiple diaphragms.

A multiple diaphragm technique is very useful as a "breaker" mechanism which is independent of external control when pressure burst diaphragms are used. However, such a technique is inflexible in the choice of pressure ratios and pressure differentials causing bursts (ΔP), which may be used without a deterioration in performance. This is a result of the fact that the maximum pressure differential is re-lated to the pressure ratio. The deterioration of performance is markedly greater when diaphragms with equal burst pressures are used. To obtain the results described in most literature, diaphragms with burst pressures of specific and different values for each set of operating conditions must be used.

For a double diaphram shock tube two possible wave phenomena exist. They are:

> (a) The shock from diaphragm one proceeds to diaphragm
>
> two, increasing the stagnation property values and

giving the disturbed gas a velocity increment.
Then, diaphragm two is broken externally as the
shock impacts, with no reflected shock.

(b) The shock from diaphragm one strikes diaphragm two
and a reflection of the shock and subsequent cancel-
lation of the velocity increment occurs. This
causes a further increase in stagnation quantities.
In this case, diaphragm breakage results from the
impacting shock pressure.
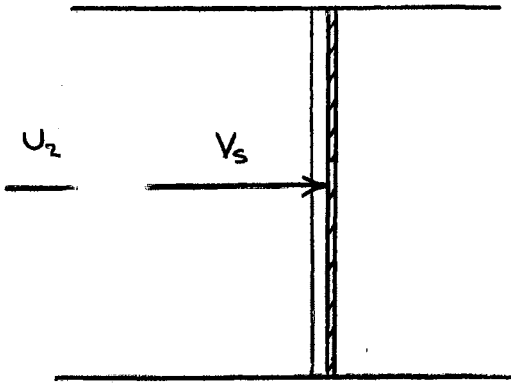
Non-reflected Case
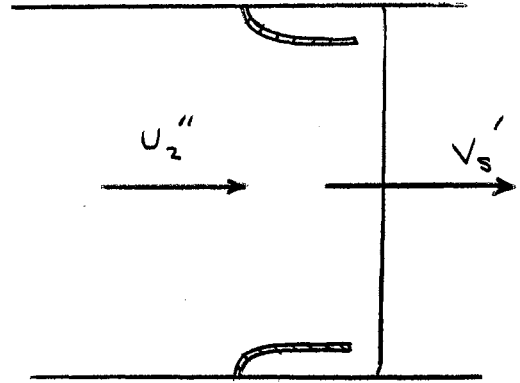

Figure 19. Impacting Shock

Figure 20. Resultant Shock.

Transforming A-6, the flow conditions existing after the second diaphragm breaks, into a stationary shock yields the following figure.
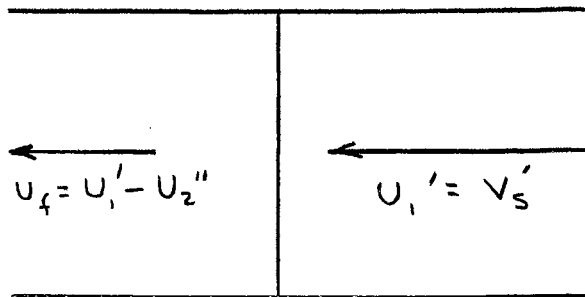

Figure 21. Transformation to Standing Shock.

Now $U_2'' \doteq U_2 + U_2'$ where U_2' is the velocity which would occur if a second shock tube with stagnation conditions equal to those behind the shock.

So,

(14) $\qquad U_f \doteq U_1' - U_2 - U_2' = U_1'(1-\dfrac{U_2'}{U_1'}) - U_2$

Substituting (3) and (4) into (14) gives:

(15) $\qquad U_f = \dfrac{a_1'}{\gamma_1'}\left(\dfrac{P_2'}{P_1'}-1\right)\left[\dfrac{2/\gamma_1}{\left(P_2'/P_1' - \dfrac{\gamma_1-1}{\gamma_1+1}\right)}\right]^{\frac{1}{2}} - U_2$

Downstream of the diaphragm (7a) applies, so equating (15) and (7a) and simplifying gives:

(16) $\qquad \dfrac{P_4'}{P_1'} = \dfrac{P_1'}{P_2'}\left\{\dfrac{a_1}{\gamma_1}\left[\left(\dfrac{P_1}{P_2}\right)^{-\frac{\gamma_4}{\gamma_4+1}} - 1\right]\right.$

$\qquad\qquad \left.\left[\dfrac{2/\gamma_1}{\dfrac{P_2'}{P_1'}(\gamma_1+1) + \gamma_1 - 1}\right]^{\frac{1}{2}} + \dfrac{2a_4'}{\gamma_4-1}\right\}^{-\frac{\gamma_4+1}{2\gamma_4}}$

The following steps may be followed to arrive at tabular values of final Mach number versus overall pressure ratio for the non-reflected case.

(1) Calculate shock Mach number for various driver-to-driven pressure ratios (SM = SM(RATIO) in IBM program given in this paper)

(2) Read values of Mach number for the pressure ratios

desired

(3) Calculate $\dfrac{P_2'}{P_1'} = \dfrac{P_3}{P_i} = 1 + 1.25\,(M_s^2 - 1.0)$ for the values chosen

above, where P_i is intermediate pressure.

(4) Calculate P_3 from the following relation.

$$P_3 = \dfrac{P_3}{P_i}\,\dfrac{P_i}{P_4}\,P_4 = \dfrac{P_3}{P_i}(P_4 - \Delta P)$$

(5) Use P_3 as stagnation pressure for the second diaphragm

burst. This assumes that $\dfrac{U_2}{a_1}$ is relatively small. $\left(\dfrac{U_2}{a_1} < 0.5\right)$.

(6) Calculate

$$T_3 = T_1\;\frac{\dfrac{P_3}{P_i}\left[1 + \left(\dfrac{\gamma-1}{\gamma+1}\right)\dfrac{P_3}{P_i}\right]}{\dfrac{P_3}{P_i} + \dfrac{\gamma-1}{\gamma+1}}$$

for each selected value of P_3/P_i.

(7) Calculate $a_3\sqrt[2]{\gamma_3 g R T_3}$.

(8) Use the values obtained in (7) in equation (16) to obtain

P_3/P_1.

(9) Correct values of $\dfrac{P_3}{P_1}$ obtained from step (8) to $P_4/P_1 =$

$(P_3/P_1)(P_4/P_3)$ for selected conditions.

SECTION III

Reflected Case

The following procedure may be used to investigate the performance of a multiple diaphragm pressure burst shock tube in which the following events occur.

(1) The first diaphragm breaks.

(2) A shock is formed immediately and proceeds downstream.

(3) The shock strikes the second diaphragm breaks just after the reflection occurs. This break is a result of the pressure differential across the diaphragm.

The value of the Mach number of the first shock formed (M_1) is a function of the gases used and the temperature and pressure ratios across the diaphragm. Values of M_1 for many combinations have been plotted versus the pressure ratio (P_4/P_1) in many references. Equation (16) may be used to calculate values of M_1 implicitly.

Selecting values of P_4/P_i $(P_i = P_{intermediate})$ and utilizing equation (17), allows the calculation of values of P_4 within structural limitations.

$$(17) \quad P_4 = P_1 + \Delta P \quad \text{where } \Delta P = \text{pressure differential}$$

Initially, the gas in the driven section has zero velocity and known pressure and temperature values. As the first shock passes through the gas it increases the values of temperature and pressure and causes a velocity increment. The return passage of the reflected shock causes further increases in pressure and temperature, but cancels the velocity increment.

Denoting conditions behind the first shock with a prime (') and conditions behind the second shock with a double prime (") gives the following relations.

$$(18) \quad U_2' = \frac{2a_1}{\gamma_1+1} \left(M - \frac{1}{M_1} \right) + U_1 \overset{o}{\text{ initially}} \qquad U = \text{velocity of gas}$$

$$(19) \quad a_2' = a_1 \left\{ 1 + \frac{2(\gamma_1-1)}{(\gamma_1+1)^2} \left[\gamma_1 M_1^2 - \left(\frac{1}{M_1}\right) - \gamma_1 + 1 \right] \right\}^{\frac{1}{2}}$$

$a \equiv$ velocity of sound

$$(20) \quad P_2' = P_1 \left[1 + \frac{2\gamma_1}{\gamma_1+1} (M_1^2 - 1) \right]$$

$$(21) \quad \frac{U_2'}{a_2'} = \frac{2}{\gamma_1'+1} \left(M_1' - \frac{1}{M_1'} \right) \Rightarrow M_1' \equiv \text{reflected shock Mach number}$$

$$(22) \quad P_2'' = P_2' \left[1 + \frac{2\gamma_1'}{\gamma_1'+1} (M_1'^2-1) \right]$$

$$(23) \quad a_2'' = a_1' \left\{ 1 + \frac{2(\gamma_1'-1)}{(\gamma_1'+1)^2} \left[\gamma_1' M_1'^2 - \left(\frac{1}{M_1'}\right)^2 - \gamma_1' + 1 \right] \right\}^{\frac{1}{2}}$$

$$(24) \quad T_2'' = \left(\frac{a_2''}{a_1} \right)^2 T_1$$

Using values of T_2'' and P_2'' as the stagnation quantities for the second

diaphragm in equation (16) results in a listing of final shock Mach

number versus the pressure ratio across the second diaphragm. Equation

(25) may then be used to obtain the overall pressure ratio.

$$(25) \qquad \frac{P_4}{P_1} = \left(\frac{P_4}{P_2''} \right) \left(\frac{P_2''}{P_1} \right)$$

The results may be plotted as M_{final} versus $(P_4/P_1)_{overall}$.

APPENDIX B

APPENDIX B

1620 IBM FORTRAN PROGRAM FOR SINGLE DIAPHRAGM CASE

GA   =   Specific heat ratio of driven gas

GB   =   Specific heat ratio of driver gas

TA   =   Temperature of driven gas

TB   =   Temperature of driver gas

AMA   =   Molecular weight of driven gas

AMB   =   Molecular weight of driver gas

SM   =   Shock Mach number

DEL   =   Variation in SM

```
1   READ, GA, GB, TA, TB, SM, AMA, AMB, DEL

    A    =  ((GB*AMA*TB)/(GA*AMB*TA))**0.5

2   B    =  (GA-1.0)*(((((2.0*GA)/(GA-1.0))*(SM**2))-1.0)/(GA+1.0)

    C    =  ((GB-1.0)*((SM**2)-1.0))/((GA+1.0)*A*SM)

    D    =  (2.0*GB)/(1.0-GB)

    RATIO =  B*((1.0-C)**D)

    CSA  =  ((GA*32.17*1545.0*TA)/AMA)**0.5

    V    =  SM*CSA

    PUNCH, SM, RATIO, V

    SM   =  SM+DEL

    IF(RATIO-200.0)2, 2, 3

3   GO TO 1

    END
```

APPENDIX C

APPENDIX C

To provide a short intense burst of light at accurately timed intervals
the following multiple light source, originally designed by Cornell
Aeronautical Laboratory, was constructed. Basically, the system consists
of a structure to hold five spark gaps in a fixed line and an electronic
circuit to provide a quick discharge of a capacitor across the spark gaps.

Figure 22 shows a cross sectional view of one of the spark gaps
and the capacitor used to drive it. A photograph of the entire unit is
given in the equipment section of this paper (Plate IV).

Each spark gap unit was focused through a 34 millimeter diameter
and 66 millimeter focal length lens in such a manner that all the spark
sources appeared to be at a single point. Extreme care was taken to
insure that the units did focus from a single point. To insure this a
mono-filament light was placed at the end of the assembly and each unit
was focused in turn. A general view of lens system is shown in Figure
23.

The cylindrical capacitors used to provide the electrical energy for
each spark gap was made of barium titanate (ϵ = 1500) and were furnished
in a smooth, ground condition by Solidtronics Inc., of Santa Barbara,
California. The dimensions of the cylinders were obtained from an
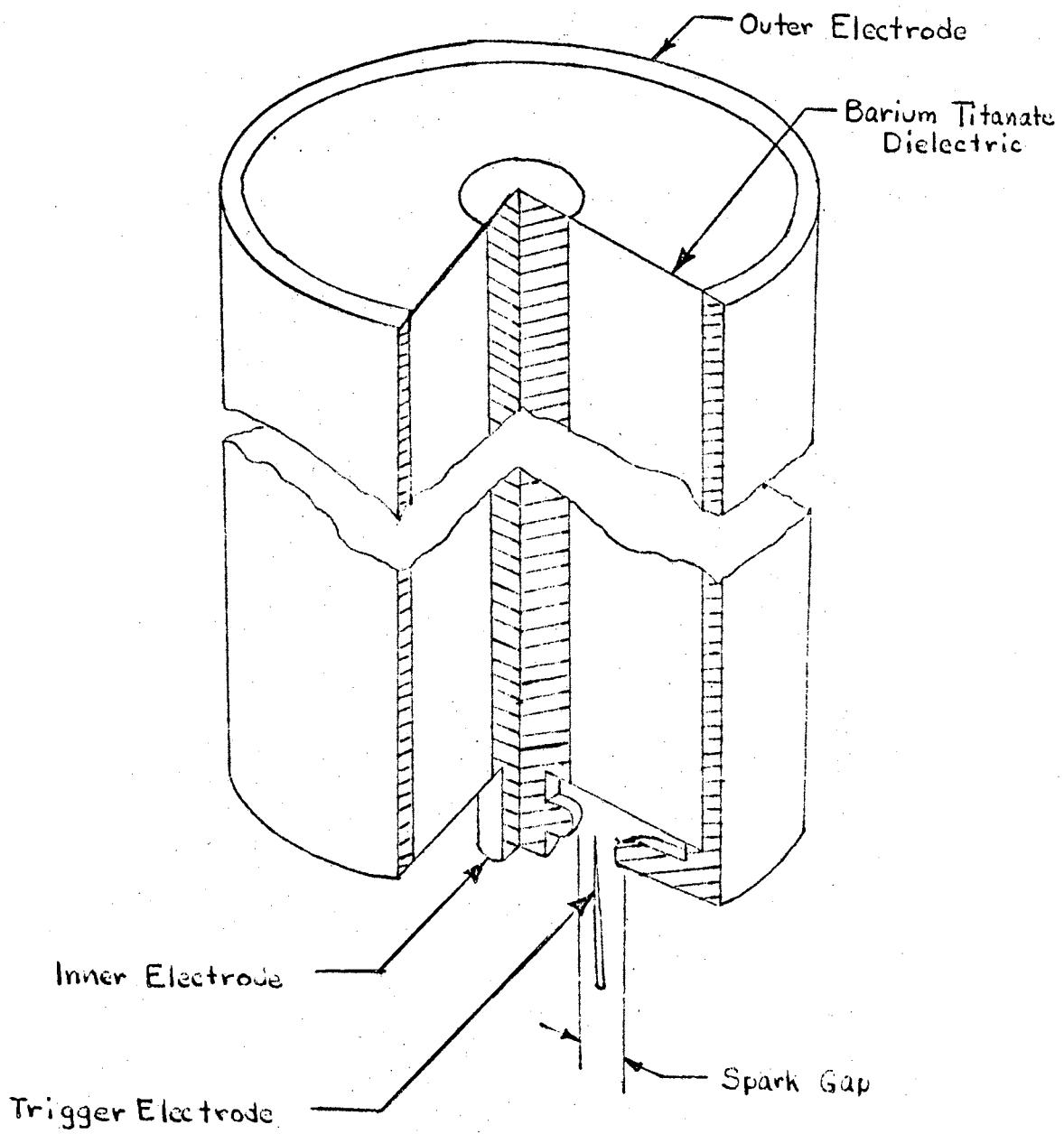analysis of capacitor design as given by Fitzpatrick, Hubbard, and
Thaler (11).

81

Outer Electrode

Barium Titanate Dielectric

Inner Electrode

Trigger Electrode

Spark Gap

Figure 22. Cross Sectional View of Capacitor Unit.

To shock tube
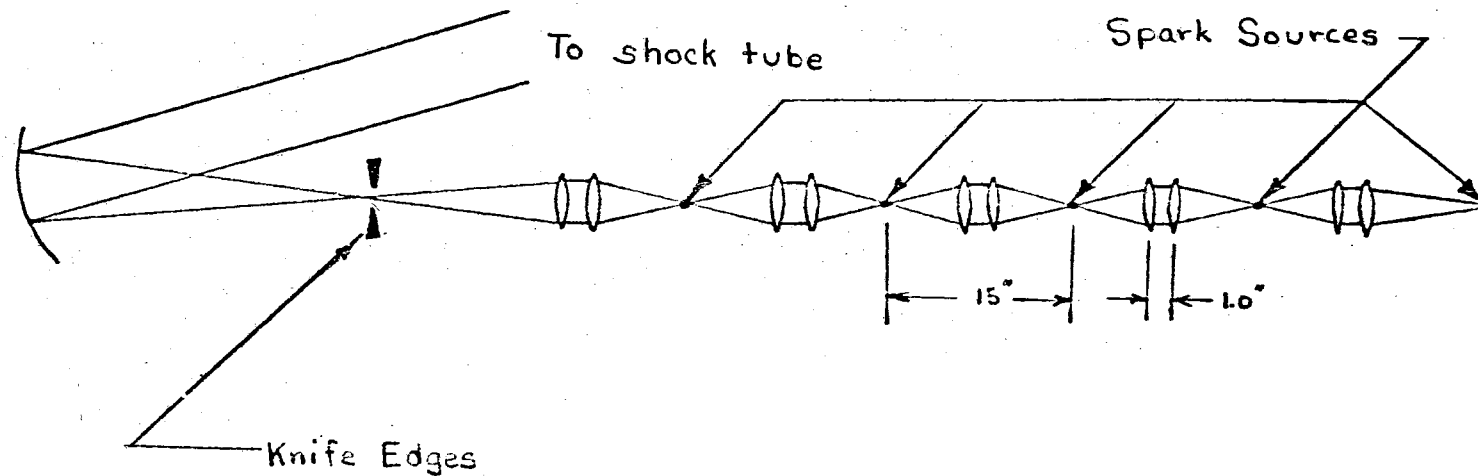
Spark Sources

Knife Edges

15" 1.0"

Figure 23. Lens System.

The capacitance of the barium titanate cylinders is 0.25 micro-farads. The spark gaps may be set at varying distances depending on the humidity of the air, which effects standoff distances. The distances were sufficient to hold off about 12,000 volts.

Power to the units was furnished by an Industrial Instruments, Inc. Molded Rock 10 kilo-volt, 5 milli-amp regulated power supply. The units were charged in parallel through a 220 K-ohm resistor and separated by a gang switch. The triggers to the spark gaps were provided by a trigger electrode set close to the ground side of the spark gap. When a pulse of sufficient voltage was impressed on the trigger electrode the total resistance gap of the spark gaps was reduced to a value less than that necessary to hold off 10,000 volts.

To provide an accurately timed pulse to the trigger electrode the following circuit was devised.

(1) A Kistler 701 pressure transducer is used to provide an initial pulse.

(2) This pulse is amplified by a Kistler 568 charge amplifier.

(3) The resulting signal is amplified by the preamplifier of a Tektronix 535A oscilloscope.

(4) This signal is then applied to an Engineered Electronics Z-8889 one-shot multi-vibrator, which had been slightly modified.

(5) The out put of the Z-8889 is used to drive the grid on a hydrogen thyratron (3C45/6130) power tube.

(6) When this tube begins to conduct it causes a
voltage to be impressed on the center tap of a
Stancor 6426 photo-flash trigger coil.

(7) The reactance of the coil then causes a high
voltage pulse to be applied to the trigger electrode,
resulting in the discharge of the main capacitor
across the spark gap.

Complete schematics of each component and of the entire unit are
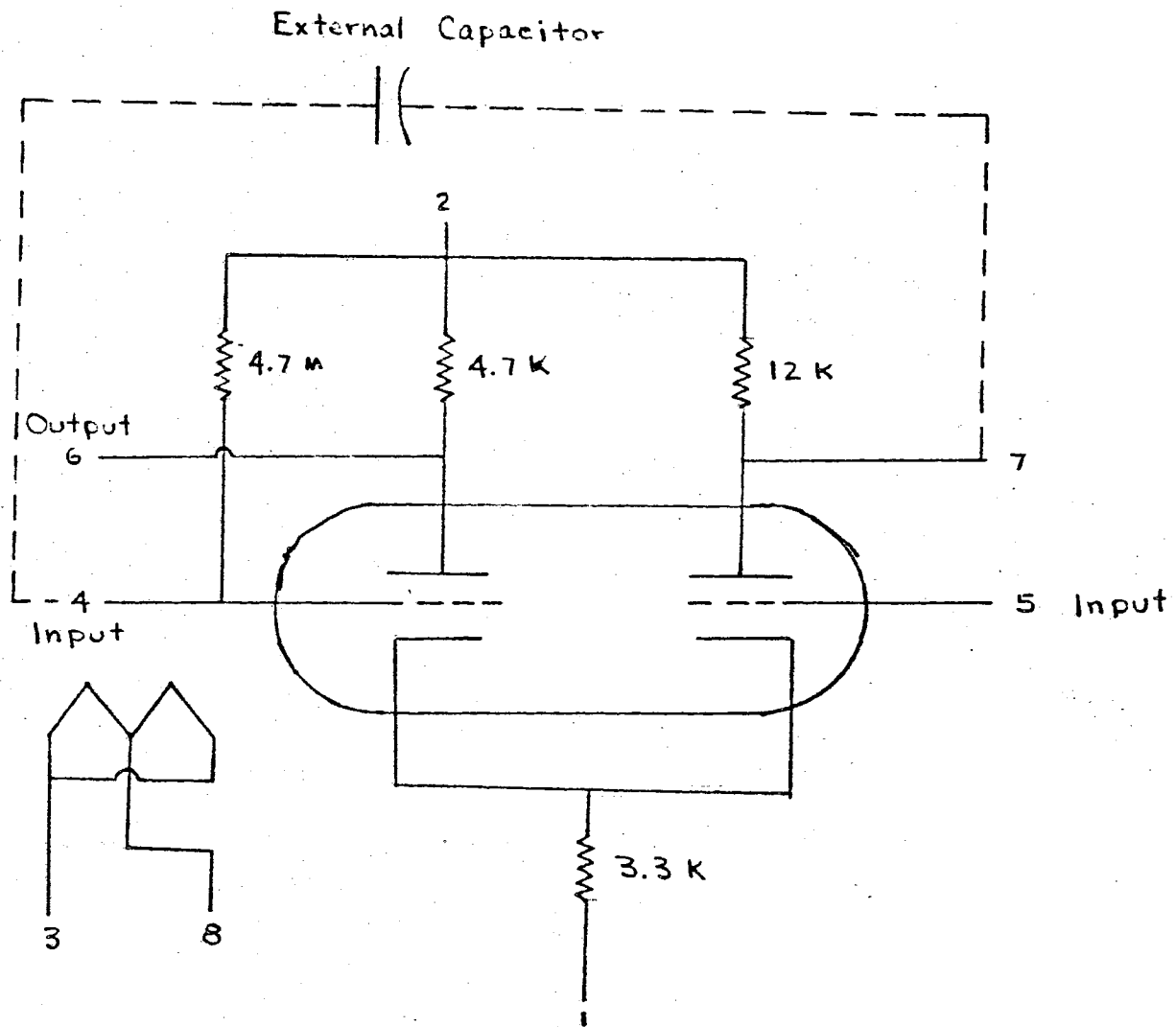shown in the following Figures: 24, 25, and 26.

Figure 24. Schematic of Multivibrator.

Pin 1- Heater
Pin 2 - Cathode, Returns
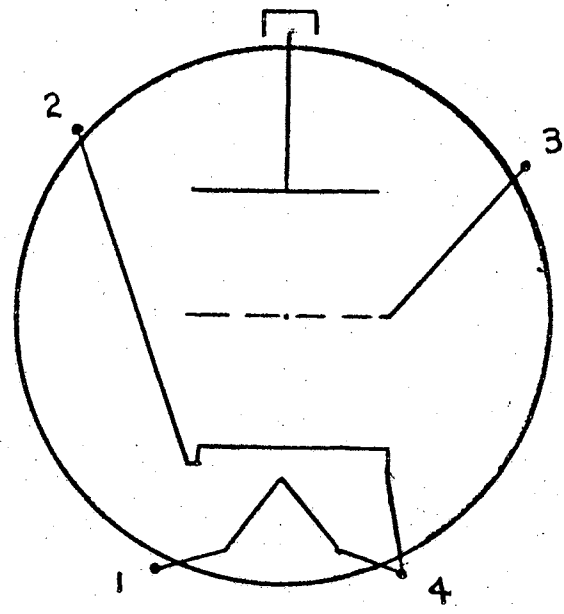Pin 3 - Grid
Pin 4- Heater, Cathode
Cap - Anode
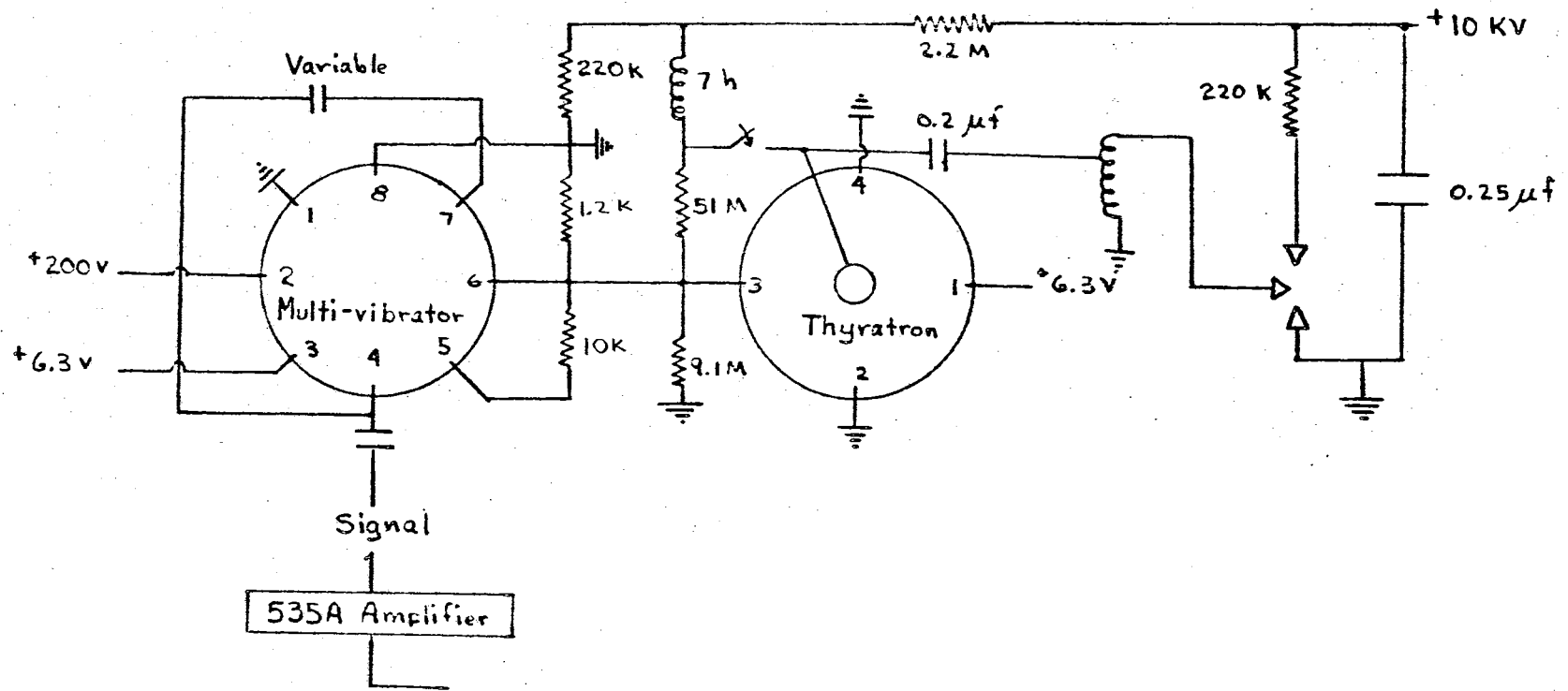
Figure 25. Schematic of Thyratron.

Figure 26. Schematic of Entire Unit.

VITA

Glendon Ray Lazalier

Candidate for the Degree of

Master of Science

Thesis: DESIGN AND CONSTRUCTION OF A SHOCK TUBE FACILITY FOR THE STUDY OF SHOCK WAVES EMERGING FROM OPENINGS

Major Field: Mechanical Engineering

Biographical:

Personal Data: Born in Heavener, Oklahoma, August 20, 1941, the son of Carl G. and M. Verdine Lazalier.

Education: Attended Heavener public schools and graduated from Heavener High School in 1959; received the Bachelor of Science degree from the Oklahoma State University with a major in Mechanical Engineering (Aeronautical Option), in May, 1963.

Professional Experience: Employed from June, 1962 to September, 1962, as a student engineer with American Telephone and Telegraph Corporation in Oklahoma City; employed from June, 1963 to September, 1963 as an associate engineer with Chevrolet Engineering Center in Warren, Michigan; employed June, 1964 to September, 1964 with Douglas Aircraft Co., Inc., at Tulsa as an associate engineer.